Himmat Gill

High Power Wireless Transfer

For Charging High Power Batteries

Helsinki Metropolia – University of Applied Sciences

Bachelor of Engineering

Electronics

Thesis

September 2017

Author	Himmat Gill
Title	High Power Wireless Transfer
Number of Pages	44 pages + 3 appendices
Date	11 September 2017
Degree	Bachelor of Engineering
Degree Programme	Electronics
Instructor	Kai Lindgren; Senior Lecturer

Wireless power transfer (WPT) is developing with emerging of new technologies that has made it possible to transfer electricity over certain distances without any physical contact, offering significant benefits to modern automation systems, medical applications, consumer electronic, and especially in electric vehicle systems.
 The goal of this study is to provide a brief review of existing compensation topologies for the loosely coupled transformer.

The technique used to simulate a contactless power transfer system is based on Finite Element Method or Analysis (FEM or FEA) coupled with electric circuits provided by COMSOL Multi-Physics simulation software. The task was to provide an innovative technique for high power wireless transfer with a power output ranging from 15 to 20 [kW]. Analyses were conducted with the input of zero phase angle of the supply voltage. A passive resonant network used to achieve constant (load-dependent) voltage or current output was summarized. Furthermore a simple circuit model was also simulated using National Instruments Multisim software to analyse the results.

Overall the results generated by the simulation software were at par with what was anticipated after building a mathematical model based on numerical calculations. Anyhow we were not able to build a physical working model but using the software various models were simulated with different parameters before reaching a conclusion.

Keywords	Contactless Power Transfer (CPT) Inductive Power Transfer (IPT)

Helsinki Metropolia University of Applied Sciences

Contents

1.   Introduction

The study subject for this project was provided by KONE, to innovate or research about a high power contactless or wireless power system. This technology, if found suitable as per their requirements, would be adopted and implemented in their field of business to improve the way elevators are operated in a building.

Wireless power transfer has become a popular academic research subject in recent years with quite interesting prototypes being invented across different universities worldwide. Even some new companies venturing into this field of business have experienced a significant growth. The main principle of operating a contactless power transfer revolves around the working principle of a transformer, since it involves coils in different shapes and sizes. The way electricity is transferred between coils is through electromagnetic induction. An electric field produces a magnetic field, which are perpendicular to each other, and vice a versa. The higher the current passing through a conductor or a wire or a loop (a strong electric field), the stronger will be the magnetic field which would induce an electric current in another wire or loop or coil within its intensity field. To make this system work efficiently there should be an electromagnetic resonance between the coils or wire loops placed in close vicinity to one another. This is where power electronics circuitry plays an important role in creating a resonant coupling between the coils or wire loops used for contactless power transfer.

Power electronics involves assembling of resonant capacitors and inductors whether in series or parallel to each other, so as to achieve a resonant frequency where the two adjacent circuits are matched and operate together in harmony. Resonant frequency can be calculated using the mathematical model as mentioned in appendix 2, and the required electronic components can be assembled to make a wireless power transfer efficient. In this project a high power output was desired, in kilowatts [kW], which was hard to implement in the university laboratory, hence the model was simulated using COMSOL Multi-Physics simulation software.

A simple ideal transformer was designed without considering the resonance coupling to transfer power from the primary cable to the secondary coil in this model following the principles of electromagnetic induction and the behaviour of a transformer. All the necessary mathematical calculations were completed to replicate similar results when the model was simulated. Table 1 lists all the variables representing various elements of electromagnetism used in the numerical equations mentioned in this study.

Table 1: List of all the variables used in the mathematical equations and calculations.

Φ_B	Magnetic Flux. $Units \rightarrow \left[\dfrac{Nm}{A}\right]$
Units of Φ	$Weber[Wb]$ or $Weber.Turns\,[WbTurns]$ in case of Flux Linkage
N_P	Number of Turns in Primary Coil [Cable]
N_S	Number of Turns in Secondary [Coil] $=$ [Windings]
I_P or I_1	Current in Primary Cable
I_S or I_2	Current in Secondary Coil
Λ	Magnetic Permeance
μ_r	Relative Permeability
Soft Iron Core	Ferrite (Nickel Zinc). $\mu = 2*10^{-5}to\ 8*10^{-4}$ $\mu_r = 16\ to\ 640.\ Assumed\ to\ be\ 200\ for\ this\ model.$
μ_0	Vacuum Permeability $\approx 4\pi*10^{-7}\left[\dfrac{H}{m}\right]$ or $\left[\dfrac{N}{A^2}\right]$
B_{MAX} or B_{SAT}	Magnetic Flux Density or Magnetic Field Strength. Core's onset of Saturation from Primary Current - I_P
Units of B	$Tesla\,[T] \rightarrow 1[T] = 1\left[\dfrac{N}{Am}\right] = 1\left[\dfrac{Weber}{m^2}\right] = 10000[Gauss]$
l_m or l_{MIN}	Magnetic Path Length or Circumference of the inner boundary of the Magnetic Core cylindrical in shape. For a square shaped Magnetic Core each side $\rightarrow\ s\ =\ \dfrac{l_{MIN}}{4}$
A_C	Cross Sectional Area
r_P	Radius of the Primary Cable
V_P or V_1	Supply Voltage (Primary Cable)
E_P	Induced Primary Voltage
V_S or V_2	Output Voltage (Secondary Coil)
E_S	Induced Secondary Voltage
P_P	Input or Supply Power (Primary Cable)
P_S	Output Power (Secondary Coil)
a	Voltage Ratio or Winding Turns Ratio
Z_L	Load or Secondary Impedance
L_P or L_1	Transformer Primary Coil Inductance
L_S or L_2	Transformer Secondary Coil Inductance

2. Theoretical background

2.1. Transformers

Transformers are one of the most basic yet practical devices used in Alternating Current (AC) systems from power generating plants to a simple doorbell and are usually represented in an electric circuit as shown in figure 1. They are used to increase (Step-up) the voltage to be supplied over long distance power lines and then subsequently reduce (Step-down) the voltage before distributing electricity to houses and buildings. Electrical energy is transferred by a transformer using an indirect method. First it is converted into magnetic energy, and then reconverted back into electrical energy with a different voltage and ampacity or amperage. Due to this conversion process, transformers perform different functions making it an invaluable entity in the field of electricity. **[1, 3-1.]**

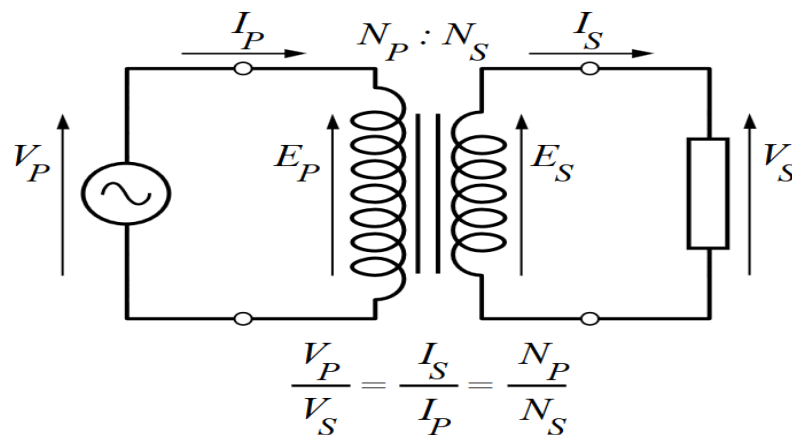$$\frac{V_P}{V_S} = \frac{I_S}{I_P} = \frac{N_P}{N_S}$$

Figure 1: Circuit schematic of an ideal transformer.

Transformers follow the principle of Mutual Induction (current flowing through a wire produces a magnetic field) as shown in figure 2 and 3, for example an electro-magnet (supplying current to an insulated wire wrapped around an iron bar induces a magnetic field in the iron bar, which acts like a magnet). This principle is also valid inversely since, a magnetic field passing through a conductor induces current in the conductor or wire. Both of these methods of inductions are used at the same time in a transformer. Mutual induction between coils can be calculated using equations (1) and (2) and to calculate the inductance of a coil independently has been explained in appendix 1.

A basic transformer consists of two separate windings of insulated wires wound around a common iron core. The power source or AC (Alternating Current) supply is attached to the primary winding, and the load to be served is attached to the secondary winding.

When the primary winding is energized an electromagnetic field builds up and then collapses in the iron core, this field cuts through the secondary coil loops inducing current and supplying power to the load attached. This power build-up and collapse is also known as the magnetic flux and occurs at a frequency of the AC supply voltage, for example with a 50 [Hz] frequency it is fifty times per second. **[1, 3-2.; 2, 1.]**
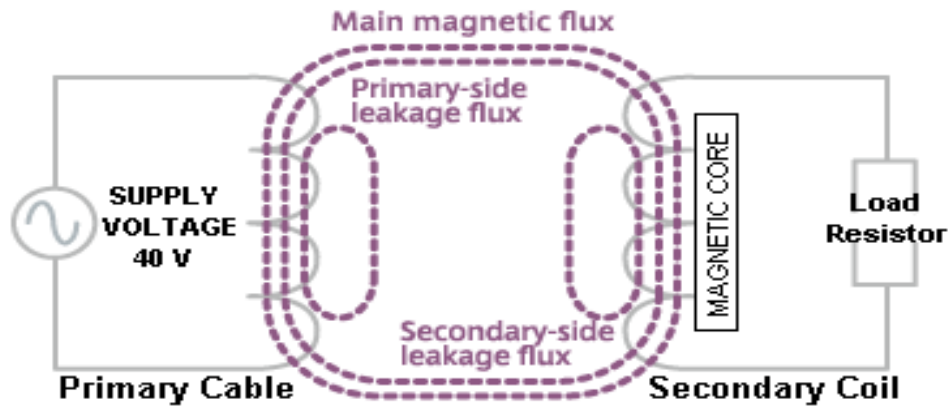

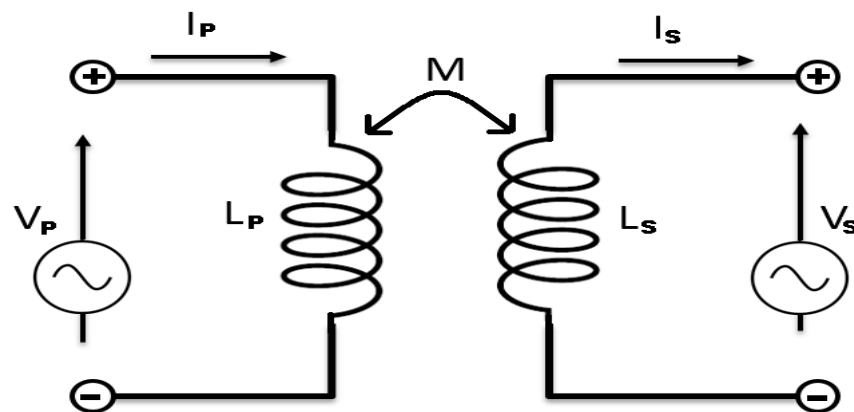Figure 2: Circuit schematic of a contactless inductive power transfer.

Figure 3: Mutual Inductance (M) between two coils.

$$Coupling\ Factor, \quad k = \frac{M}{\sqrt{L_P * L_S}}$$ (1)

$In\ an\ ideal\ case\ k = 1.$

$$Mutual\ Inductance, \quad M = k * \sqrt{L_P * L_S}$$ (2)

$$Transformer\ Ratio \rightarrow a = \frac{Primary\ Voltage\ (V_P)}{Secondary\ Voltage\ (V_S)}$$ (3)

$$Also, \quad a = \frac{Number\ of\ Primary\ Turns\ (N_P)}{Number\ of\ Secondary\ Turns\ (N_S)}$$ (4)

$$Power\ In \rightarrow V_P * I_P\ [VA]\ =\ V_S * I_S\ [W] \rightarrow Power\ Out \tag{5}$$

In an ideal transformer power-in, supplied by the primary coil, is equal to the power-out, consumed by the load attached to the secondary coil, and can be calculated using equation (5). The current in the secondary coil always changes by the inverse of the ratio by which the voltage changes. If the voltage is raised to ten times its original value by the transformer, the current in the secondary coil will be reduced to one-tenth the value of the current in the primary coil. **[1, 3-6.]**

2.2. Transformer Efficiency

The intensity of power loss in a transformer determines its efficiency which is reflected in power (Wattage) loss between the primary winding (input power in Volt Ampere) and secondary winding (output power in Watts). It can be calculated using equations (9).

$$Efficiency\ or\ Power\ Factor = \frac{Output\ Power\ [W]}{Input\ Power\ [VA]} \tag{6}$$

$$Efficiency\ of\ a\ transformer, \quad \eta = \frac{Output\ Power}{Input\ Power} * 100\% \tag{7}$$

$$Also, \eta = \frac{Input\ Power - Losses}{Input\ Power} * 100\% = 1 - \frac{Losses}{Input\ Power} * 100\% \tag{8}$$

$$V = N * \frac{d\Phi}{dt}\ [Volts] \tag{9}$$

Transformer voltage either on the primary or secondary side can be calculated using equation (9) which is the product of the rate of change of magnetic flux and the number of turns on either side respectively.

2.2.1. Eddy Currents – are local short-circuit currents induced in the iron core by alternating magnetic flux. They circulate in the core and produce heat. This can be minimized by slicing the core into thin laminated layers. Magnetic core materials are reasonably good conductors of electric current. Hence, according to Lenz's law, magnetic fields within the core induce to flow within the core. The eddy currents flow such that they tend to generate a flux which opposes changes in the core flux Φ*(t).* The eddy currents tend to prevent flux from penetrating the core as shown in the following figure 4. **[3, 39.]**
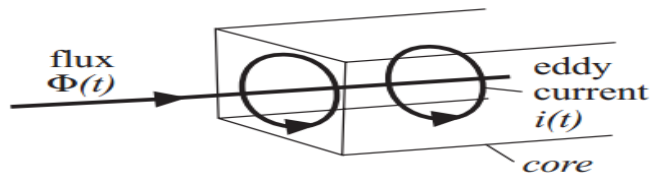
Figure 4: Eddy Current Losses $= \mathbf{i^2}(t)*$*[Resistance of the core material]*

2.2.2. Hysteresis – is the lagging of the magnetic molecules in the core in response to the alternating magnetic flux. This lagging (or out-of-phase) condition is due to the fact that it requires power to reverse magnetised molecules which do not reverse until the flux has attained sufficient force to reverse them. Their reversal generates friction producing heat in the core, which is a form of power loss. It is minimized with the use of special steel alloys which are annealed properly. Magnetic core material characteristics can be represented using a B and H curve graph as shown in figure 5 and 6 below.
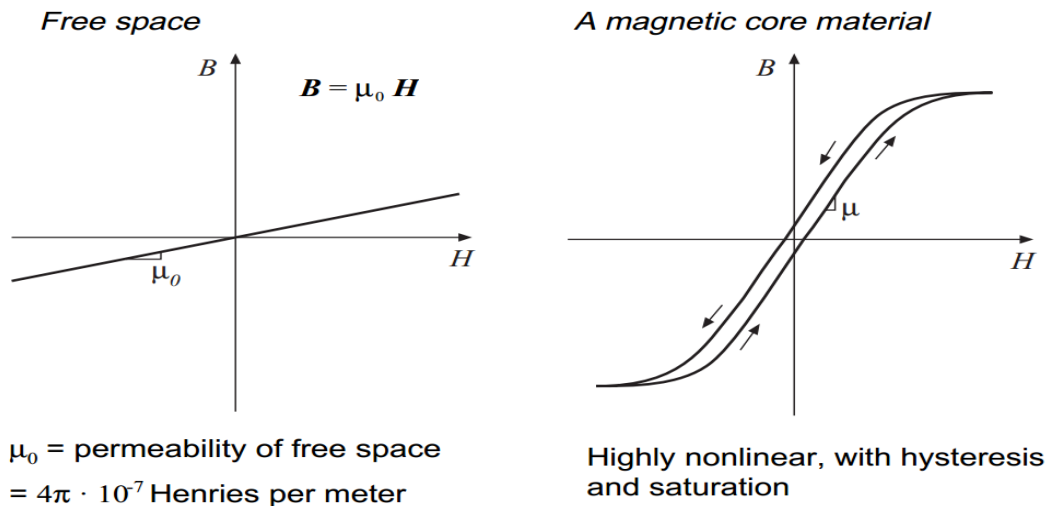

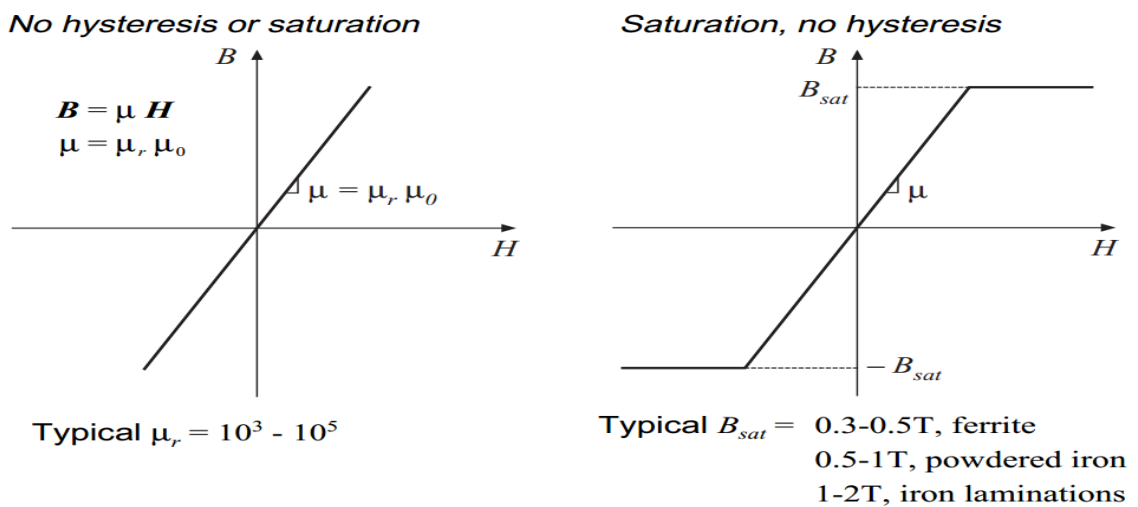Figure 5: The relationship between *B (Magnetic Flux Density)* and *H (Magnetic Field)*

Figure 6: Piecewise-linear modelling of core material characteristics. **[4, 9-15.]**

2.2.3. I²R Loss – is the power lost in circulating current in the windings, also referred to as "copper loss". This represents the greatest loss in the operation of a transformer, and can be determined (in each winding) by squaring the current and multiplying with the resistance of the winding. **[4, 42.]** Direct Current (DC) resistance of a wire or a coil can be calculated using equation (10).

$$R_{DC} = \rho * \frac{l_W}{A_W} \tag{10}$$

Here,
$l_W \rightarrow Length\ of\ the\ wire\ or\ coil$
$A_W \rightarrow Wire\ (bare)\ or\ coil\ (radius) cross-sectional\ area$
$\rho = 1.724 * 10^{-6}[\Omega.cm] \rightarrow Resistivity\ of\ soft\ annealed\ copper\ at\ room$
$\quad temperature\ (around\ 25°C) which\ increases\ to\ 2.3 * 10^{-6}[\Omega.cm]\ at\ 100°C.$

2.2.4. Power Factor – Transformers are composed of coils that behave like an inductor. The magnetic effect produced by the coil on applying power, oppose the current flow which starts to lag behind the voltage, making them appear out of phase. This phenomenon is called inductance, which causes a type of resistance in the electrical circuit hence reducing the current output. **[1, 3-9.]**

Another interesting feature of a transformer which is widely applied is known as transformer tapping and can be visually understood by looking at figure 7. It is a way to derive different output voltages by tapping into the secondary winding at various locations. Tapping is also sometimes built into the primary side (winding) as well where the supply voltage can be controlled. This is helpful when different voltage levels are required by different loads attached to the secondary output.
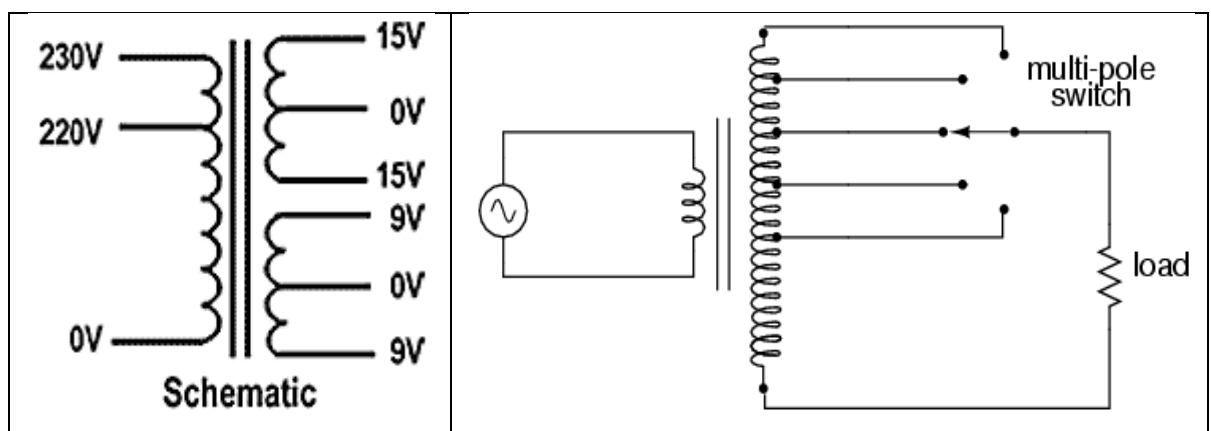

Figure 7: Circuit schematic of transformer tapping. **[5, 1].**

2.3.   Current Transformer [CT]

It is a type of an instrument transformer which is used to convert a primary current into a secondary current through a magnetic medium. Its secondary winding then provides a much reduced current which can be used for detecting over-current, under-current, peak current, or average current conditions. Figure 8 illustrates the basic components of a current transformer and their functional mechanism.
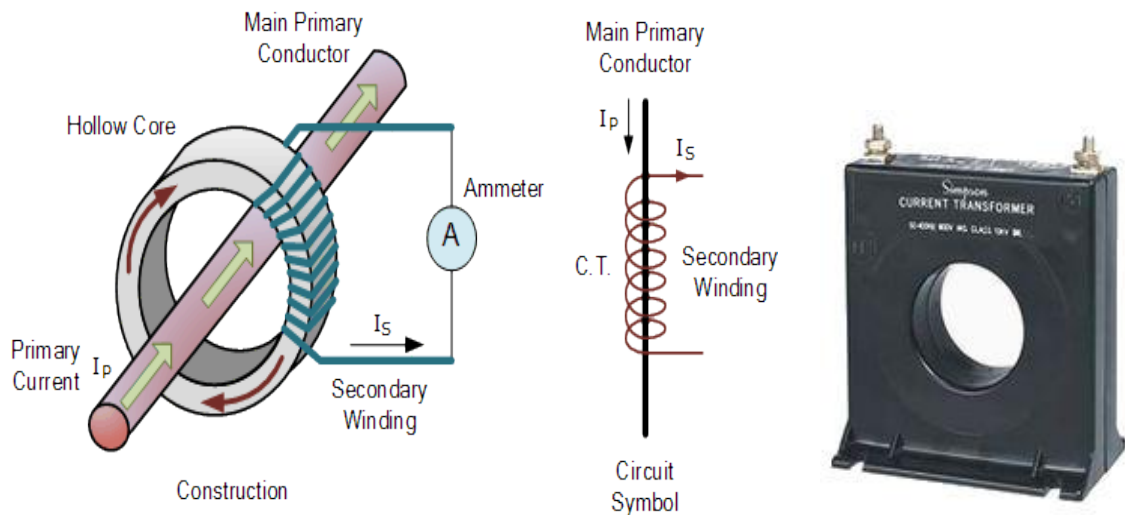

Figure 8: Current transformer basic structure.

Current transformers reduce high voltage currents to a much lower value and provide a convenient way of safely monitoring the actual electrical current flowing in an AC transmission line using a standard ammeter. The principal of operation of a basic current transformer is slightly different from that of an ordinary voltage transformer.

A current transformer's primary coil or wire, as shown in figure 9, is always connected in series with the main conductor (secondary coil winding inside the grey coloured square toroidal core) and is also referred to as a series transformer. Primary coil construction can be one single turn or a few round turns, usually for low current ratios.
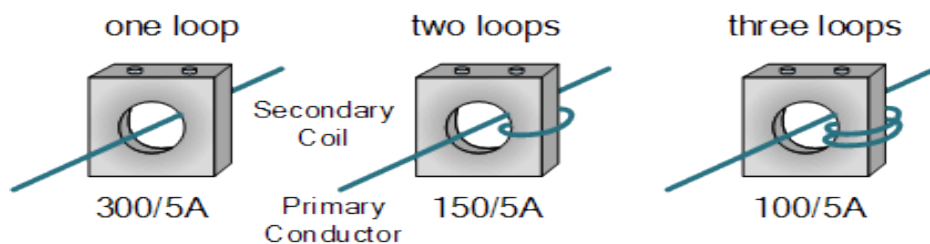

Figure 9: Current Transformer Primary Turns Ratio. **[6(a), 1.]**

There are three basic types of current transformers as follows:

2.3.1.   Wound Current Transformer – as shown in figure 10 the transformers primary winding is physically connected in series with the conductor that carries the measured current flowing in the circuit. The magnitude of the secondary current is dependent on the turn-ratio of the transformer.

2.3.2.   Toroidal Current Transformer – These do not contain a primary winding. Instead, the line or wire that carries the current flowing in the network is threaded through the window or hole in the centre as shown in figure 11. Some current transformers have a "split core" which allows it to be opened, installed, and closed, without disconnecting the circuit to which they are attached as shown in figure 12.

Figure 10: Wound Transformer   Figure 11: Toroidal Transformer

Figure 12: Handheld CT also known as "Clamp Meters" **[5.]**

2.3.3.   Bar-type Current Transformer – This type of current transformer uses the actual cable or bus-bar of the main circuit as the primary winding, which is equivalent to a single turn as shown in figure 13. They are fully insulated from the high operating voltage of the system and are usually bolted to the current carrying device. **[6(b), 1.]**

Figure 13: Bar-Type Transformer

Helsinki
Metropolia
University of Applied Sciences

The secondary winding supplies a current into either a short circuit, in the form of an ammeter or into a resistive load (resistance not larger than that of the ammeter), until the voltage induced in the secondary is big enough to saturate the core or cause failure due to excessive voltage breakdown. Unlike a voltage transformer, the primary current of a current transformer is not dependent on the secondary load current but instead is controlled by an external load. They reduce or "step-down" current levels from thousands of amperes down to a standard output of a known ratio to either 5 [A] or 1[A] for normal operation.

By increasing the number of secondary windings [N_S], the secondary current [I_S] becomes much smaller than the current in the primary circuit being measured, because as N_S increases, I_S decreases significantly. In other words, a current transformer satisfies the Ampere -Turn Equation as derived from equations (11) and (12).

$$Turn\ Ratio\ denoted\ by\ \rightarrow n = \frac{V_P}{V_S} = \frac{N_P}{N_S} = \frac{I_S}{I_P} \tag{11}$$

$$Hence, \quad I_S = I_P * \frac{N_P}{N_S} \tag{12}$$

It is always recommended that a current transformer should not be left open-circuited or operated without any load attached to the secondary side when there is primary current flowing through it, just as a voltage transformer should never be operated with a short circuit. If the ammeter (or load) is to be removed, it should be replaced with a very low resistor across the secondary terminals, because when the secondary is open-circuited, the iron core of the transformer becomes highly saturated producing an abnormally large secondary voltage, which could damage the insulation or deliver an electric shock if the CT terminals are accidentally touched. **[6(b), 1.]**

The idea applied in building this model is by following the working principle of a current transformer. When a high current passes through the primary cable, it produces a strong magnetic field which is intensified by the ferrite core around it. The strong magnetic field induces an electric field in the secondary coil wrapped around the core, which supplies power to the load attached to the secondary windings. Hence, there is a contactless power transfer of a high magnitude which can be converted (rectified) and used as a DC (Direct Current) source to charge high power batteries.

3.   Methods and Materials

3.1.   COMSOL Multiphysics®

It is a general-purpose software based on advanced numerical methods, which has been used comprehensively for modelling and simulating this project in a physics-based environment. With COMSOL Multiphysics, it is able to account for the magnetic coupling or the multi-physics phenomena. The software has many products to choose from to further expand the simulation platform with dedicated physics interfaces and tools for electrical, mechanical, fluid flow, and chemical applications. A 1D, 2D or 3D model can be built for simulation and computed in different domains.

3.1.1   Physics and Equation-Based Modelling Interfaces

COMSOL Multiphysics provides a significant amount of physics modelling functionality, which includes a set of core interfaces for common physics application areas such as structural analysis, laminar flow, pressure acoustics, diluted species transport, electrostatics, electric currents, heat transfer, and Joule heating. These are simplified versions of a selected set of physics interfaces available in the add-on modules. For arbitrary mathematics or physics simulations, where a preset physics option is not available, a set of physics interfaces are included for setting up simulations from first principles by defining the equations.

Several partial differential equation (PDE) templates make it easy to model second-order linear or nonlinear systems of equations. By stacking these equations together a higher-order differential equations can be modelled. These equation-based tools can further be combined with the preset physics of COMSOL Multiphysics or any of the add-on modules, allowing for fully-coupled and customized analyses. This dramatically reduces the need for writing user subroutines in order to customize equations, material properties, boundary conditions, or source terms. Also available is a set of templates for classical PDEs: Laplace's equation, Poisson's equation, the wave equation, the Helmholtz equation, the heat equation, and the convection-diffusion equation. **[7(a), 2.]**

3.1.2   Meshing and Finite Element Types

Automatic and semi-automatic meshing tools are available in COMSOL Multiphysics, including free tetrahedral, triangular and swept meshing. The default algorithm is automatic tetrahedral meshing for physics defined in solids, and a combination of

tetrahedral and boundary-layer meshing for fluids. The sequence of operations used for creating the mesh can be fully controlled by defining a mesh sequence.

A mesh sequence allows a mix of tetrahedral, prismatic, or hexahedral elements and can be made parametrically driven. In addition, when importing a mesh on one of the NASTRAN [**NA**SA **STR**ucture **AN**alysis: Finite Element Analysis (FEA) program that was originally developed for NASA in the late 1960s] formats, pyramid elements are also supported. A mesh imported on the NASTRAN format can be subsequently partitioned on the domain, boundary, and edge levels with additional coordinate-based operations. COMSOL's unique approach to multi-physics separates the geometric shape (as in 3D: tetra, prism, hex, pyramid) of the finite elements from the "finite element shape functions" providing maximum flexibility. Each geometric shape supports first, second, third, and, in some cases, higher-order shape functions, corresponding to traditional linear, quadratic, or cubic finite elements respectively.

Many types of physics utilize Lagrange finite elements, also known as iso-parametric nodal-based finite elements. This includes heat transfer, structural mechanics, electrostatics, and more. For CFD (Computational Fluid Dynamics, a branch of fluid dynamics), specialized elements and numerical stabilization schemes are also used. For vector-field electromagnetism, curved and higher-order curl elements, also known as edge or vector elements, are used. **[7(b), 4.]**

3.1.3   Convergence Plots Generated on Computing a Model

Convergence plots use graphics to show how an error estimate or time step evolves during the solution process for nonlinear, time dependent and parametric solvers. For the nonlinear solver, the convergence plots show an error estimate for each nonlinear iteration number. These numbers also appear in the Log sub-window. The segregated solver shows one plot with one graph for each segregated step. For the iterative linear system solvers, the error estimate for each linear iteration is a factor times the relative (preconditioned) residual. When these solvers are used together with the nonlinear solver, the graphs for the different linear-system solution steps are merged, and the plots use the accumulated number of iterations.

When using the parametric solver, the graphs for the different parameter steps are merged, and the plots use the accumulated number of iterations. The graphs for the different nonlinear and linear solve steps are concatenated. When using a Time-Dependent Solver, the graph shows the reciprocal of the time step size versus the time step. That is, a convergence plot with decreasing values shows that the time-dependent solver takes longer time steps, and vice versa. **[7(c), 8.]**

3.2. National Instruments Multisim – Simulation Software

National Instruments (NI) provides user friendly software, Multisim, to be able to study electrical and electronics circuits through virtual simulations. The parametric values of the components can be easily changed and the built circuit can be simulated numerous times without building any physical circuitry. As shown in figure 14, a simple model was built of the transformer circuitry and simulated which generated results, as shown in figure 15, in the virtual oscilloscope (XSC1). The blue coloured waveform is the output signal and the red coloured is the input signal. The yellow coloured boxes are the probes attached to the input and output lines, magnified in the conclusion section of the report, displaying the current and voltage levels when the circuit is activated.
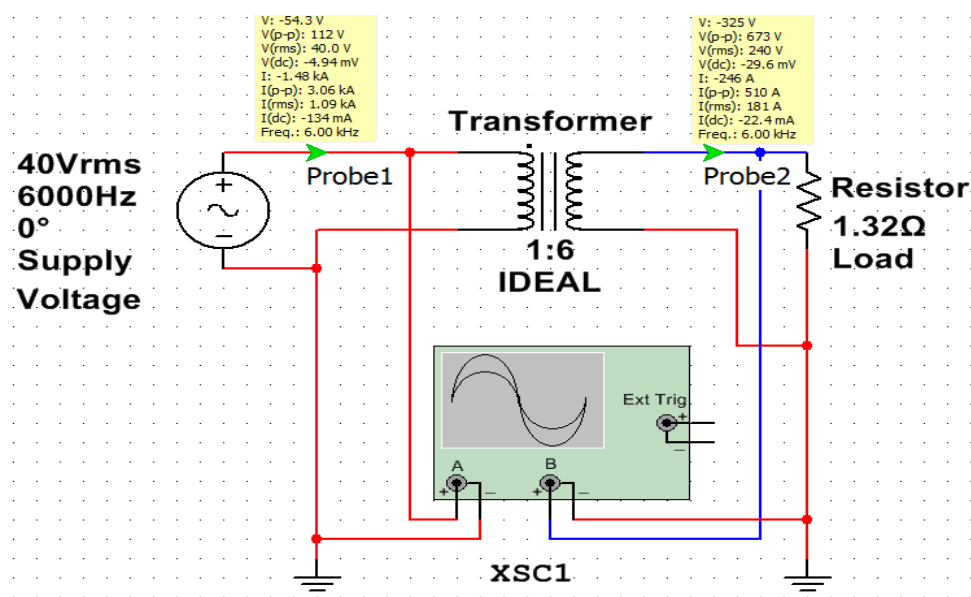
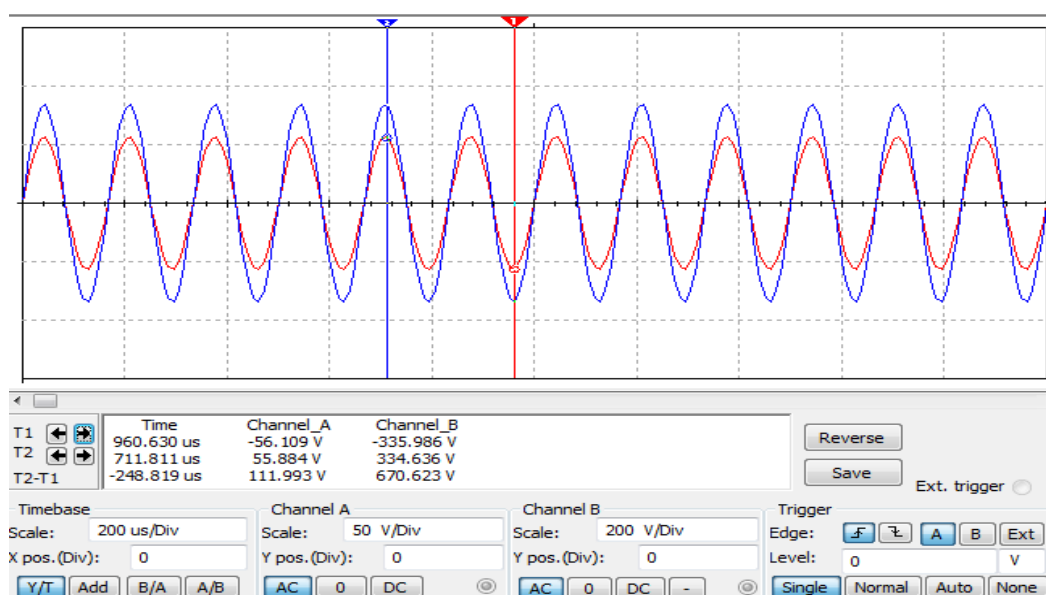Figure 14: Simulated circuit of an Ideal Transformer in Multisim

Figure 15: Simulated Oscilloscope Power-In and Power-Out graph.

3.3. Electromagnetic Induction Terminologies

3.3.1. Magnetic Field

The magnetic field at any point with a distance *r* from an infinitely long conductor carrying an alternating current with peak amplitude of I_0 and frequency **ω** (omega) can be calculated using equation (13). Where **B** is the magnetic flux density, $\mu = \mu_r * \mu_0$ - is the magnetic permeability.

$$B = \frac{\mu * I_0 * \sin(\omega t)}{2\pi r} \ [T] \qquad (13)$$

The magnitude of the magnetic flux **Φ** acting on a coil with **N** turns having a cross sectional area **A,** placed with its plane perpendicular to the magnetic field is represented as **Φ = N*B*A**, and also denoted as the Flux Linkage: **N *Φ = N*B*A = λ**

$$E \ = \ \frac{d\lambda}{dt} \ = \ N * \frac{d\Phi}{dt} \ = \ \frac{N * A * \mu * I_0 * \omega * \cos(\omega t)}{2\pi r} \qquad (14)$$

Equation (14) shows the net **voltage induced** in a coil due to the rate of change of the magnetic flux acting on it (or when a coil is placed in a magnetic field) increases proportionally with frequency, number of turns and area, and decreases proportionally with distance. It is interesting to note that the induced voltage can be increased in the coil with high relative permeability. This relationship is known as **Faraday's law**, which states that when the flux linked with a circuit changes, the induced **EMF** (Electro Motive Force) [represented by **E**] is proportional to the rate of change of the flux linkage. Similarly there is also the MMF (Magneto Motive Force) experienced by a conductor and is briefly explained in appendix 1. **[8, 25.]**

Further, if *d* is the distance between the axes of the conductors which are running parallel to each other, as illustrated in figure 16 the two wires parallel to each other but the current is travelling in opposite directions through them. And *r* is the distance of a point from mid-way between the conductors, provided *r* >> *d*, then the magnitude of the flux density can be calculated using equation (15).

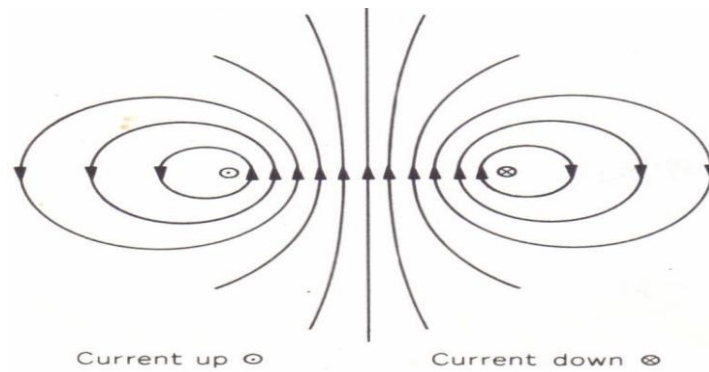$$B \approx \frac{\mu_0 * I_0 * d}{2\pi r^2} \ [T] \qquad (15)$$

Figure 16: Magnetic Field of parallel currents (cables) in opposite direction.

The **right-hand screw rule**, also known as **cork-screw rule**, associates the direction of an electric current with the direction of the magnetic force lines circling the current, also can be seen in figure 16 with the dot and cross representing the direction of current.

3.3.2 Ampere's Circuital Law

The net MMF (Magneto Motive Force denoted by F) around a closed path is equal to the total current passing through the interior of the path. For example in case of a magnetic core as shown in the figure 17, a wire carrying current $i(t)$ passing through the core window produces magnetic flux lines as illustrated with the shaded path around the interior of the core. For a uniform magnetic field strength $H(t)$, the MMF can be represented as in equation (16). When a winding consists of n – number of turns then the MMF can be calculated using equation (17). Further, at the onset of saturation due to hysteresis in the core material, the saturated current $I_{SAT} = i(t)$ can be calculated using equations (18) and (19).

$$F(t) = H(t) * l_m = i(t) \tag{16}$$

$$H(t) * l_m = n * i(t) \tag{17}$$

$$H(t) = \frac{B_{SAT}}{\mu} \tag{18}$$
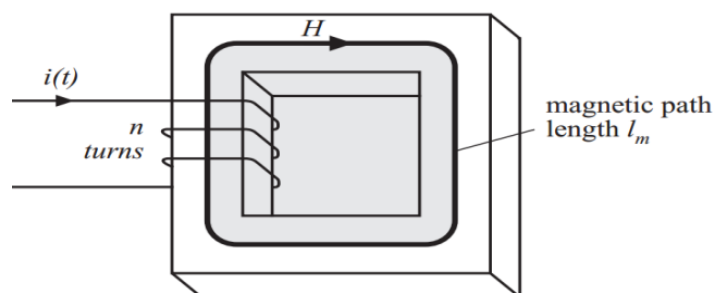
$$I_{Sat} = \frac{B_{SAT}}{\mu * n} * l_m \ [A] \tag{19}$$

Figure 17: Magnetic field generated inside the core

3.3.3 Magnetic Intensity → H

The new magnetic quantity describes the properties of the magnetic core materials and their behaviour under the influence of current. When there is no material present then *H* can be defined, as in equations (20), like in case of along straight wire. In equation (21) I_0 is the current flowing through the conductor or wire and $I_m = 2\pi r$ is the length of the magnetic path encircling in a cylindrical pattern at a distance r from the wire.

$$B = \mu_0 * H \quad \to \quad H = \frac{B}{\mu_0} = \frac{I_0}{2\pi r} \left[\frac{A}{m}\right] \tag{20}$$

$$I_0 = H * 2\pi r = H * l_m \ [A] \tag{21}$$

$$\mu_r = \frac{B}{\mu_0 * H} \tag{22}$$

When there is a presence of a magnetic core material made up of any ferrite element then, $B \neq \mu_0 * H$ instead, $B = \mu_0 \mu_r * H = \mu * H \ [T]$. Hence, the relative permeability of the core material is expressed using equation (22).

The effect of the magnetic material is to make the flux density *B* much larger than it would have been with the coil alone. Physically, this happens because the original field from the coil magnetises the material of the core. The magnetised material sets up its own field, enhancing the original field of the coil. When considering magnetic materials it is important to preserve the distinction between *B* and *H*.
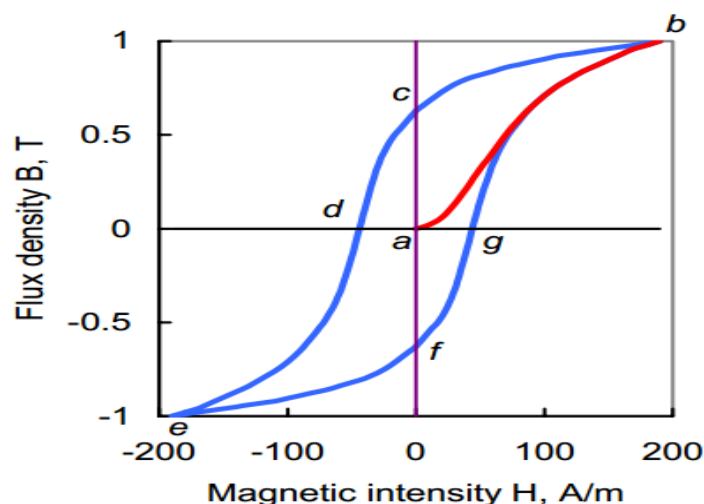

Figure 18: *B/H* Relationship derived from measurement on a ring-shaped sample (hollow cylinder) made of a soft magnetic material.

The curve *ab,* as shown in figure 18, is known as the initial *magnetisation curve* and the loop *bcdefg* is the *hysteresis loop*. The area of the loop represents energy lost per unit volume in taking the material round one cycle of magnetisation. **[8, 15.]**

4.   Results

Initially all the mathematical calculations were formulated using 6 [kHz] as the set frequency to calculate all the related parameters. Then the same frequency was used to perform the simulations in COMSOL Multiphysics, and the results were compared to conclude that the model would function practically as well.

4.1.   Mathematical Calculations

A mathematical model was built using the following values listed below in table 2 for the variables used for all the necessary calculations. The equations have been simplified so that we could easily simulate an ideal transformer behaviour.

Table 2: Approximate values used for simulation purpose considering that the model behaves like an Ideal Transformer

B_{MAX} or B_{SAT}	$1[T] = 1\left[\dfrac{Wb}{m^2}\right]$
$Ferrite\ Core - \mu_r$	$200 \rightarrow approximately$
I_P	$1000[A]$
P_P or P_S	$40\ [kW] \rightarrow desired$
V_P	$40[V]$
a	$230/40 = 5.75\ [Turns]$
V_S	$230[V]$
I_S	$40000\ [VA]/230[V] = 174[A]$
$Frequency$	$6000\ [Hz]$

4.1.1.   Calculating the Magnetic Length

It is known that magnetic flux is represented as in equation (23) and the variable Λ is the permeance of the flux as defined in appendix 3 and represented as equation (24). Then the magnetic flux density can be calculated using equation (25). Applying all the equations mentioned the magnetic length can be calculated using equation (26).

$$\Phi_B = N_P * I_P * \Lambda \tag{23}$$

$$\Lambda = \frac{\Phi_B}{N_P * I_P} = \frac{\mu * A_C}{l_m} \tag{24}$$

$$B_{MAX} = \frac{\mu * N_P * I_P}{l_m} \tag{25}$$

$$l_m = \frac{\mu_0 * \mu_r * N_P * I_P}{B_{MAX}} \tag{26}$$

Further substituting all the known values in equation (26) the value of magnetic length is calculated to be 25.133 [cm], as shown in equation (27). As the magnetic core used in the model is square shaped with round edges, and then the length of each side (inner section), denoted by s, is calculated to be 6.3 [cm] as shown in equation (28).

$$l_m = \frac{4\pi * 10^{-7} \left[\frac{H}{m}\right] * 200 * 1 * 1000[A]}{1[T] \; or \; \left[\frac{Vs}{m^2}\right] \; or \; \left[\frac{HA}{m^2}\right]} = 0.25133 \; [m] = 25.133[cm] \tag{27}$$

$$s = \frac{l_m}{4} = \frac{25.133}{4} = 6.3 \; [cm] \tag{28}$$

4.1.2. Calculating Magnetic Core Cross-Sectional Area

The magnetic flux is sinusoidal due to the alternating current supply in the primary cable and can be represented as equation (29).

$$\Phi_B = \Phi_{MAX} * sin \, (\omega t) \tag{29}$$

The relationship between the induced EMF (E_P) or the voltage induced (V_P) in a coil or cable with N_P – number of primary turns is given as, *EMF = (Number of turns) * (Rate of change of magnetic flux)*, and can be calculated using equations (30) to (34).

$$E_P \; or \; V_P = N_P \; \frac{d\Phi_B}{dt} = \; N_P * \omega * \Phi_{MAX} * cos(\omega t) \tag{30}$$

$$V_{P[MAX]} = N_P * \omega * \Phi_{MAX} \tag{31}$$

$$V_{P[RMS]} = \frac{N_P * \omega}{\sqrt{2}} * \Phi_{MAX} = \frac{2\pi}{\sqrt{2}} * f * N_P * \Phi_{MAX} \; [V] \tag{32}$$

$$E_{P[RMS]} = 4.44 * f * N_P * \Phi_{MAX} \tag{33}$$

$$V_{P[RMS]} = 4.44 * f * N_P * \Phi_{MAX} \tag{34}$$

$$\Phi_{MAX} = \frac{V_{P[RMS]}}{4.44 * f * N_P} = \frac{40}{4.44 * 6000 * 1} = 0.0015 \; [Weber] \tag{35}$$

$$A_C = \frac{\Phi_{MAX}}{B_{MAX}} = \frac{0.0015}{1} \; [m^2] \; \approx 15 \; [cm^2] \tag{36}$$

Equation (35) or (36) is also known as the Transformer EMF equation.

Since the value of the primary cable voltage is already known, the magnetic flux is calculated using equation (35).

Substituting the magnetic flux value from equation (35) in equation (36) the cross sectional area of the core material, as shown in figure 19, is calculated.
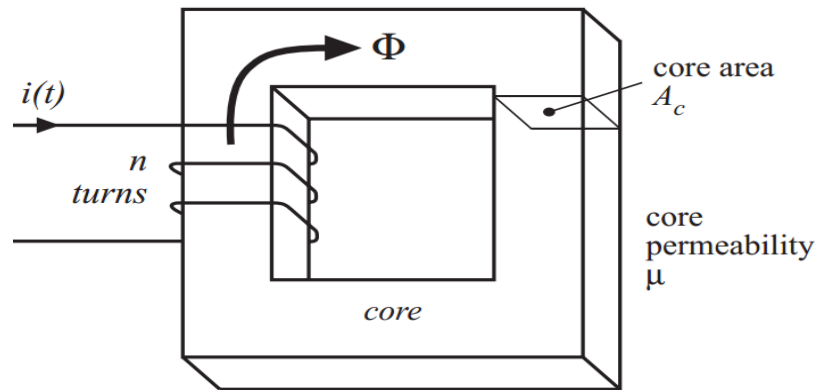

Figure 19: Representing the core cross-sectional area. [1, 5].

Another method of calculating the core cross-sectional area id by using equation (37) and is calculated in equation (38).

$$N_P = \frac{V_{P[RMS]} * 10^8}{4 * f * A_C * B_{MAX}} \tag{37}$$

$$A_C = \frac{V_{P[RMS]} * 10^8}{4 * f * N_P * B_{MAX}} = \frac{40 * 10^8}{4 * 6000 * 1 * 10000} \approx 16.67 \, [cm^2] \tag{38}$$

$Here,$

$V_{P[RMS]} \rightarrow Induced\ voltage\ in\ the\ Primary\ Cable$
$B_{MAX} \rightarrow Magnetic\ Flux\ Density\ of\ the\ core\ material\ in\ Gauss.$
$\qquad 1[T] = 10000[G]$
$A_C \rightarrow Effective\ core\ cross\ sectional\ area.$
$\qquad A_C = Height * Width(of\ the\ core)[cm^2]$
$\Phi_{MAX} \rightarrow Maximum\ Magnetic\ Flux\ in\ Webers\ [Wb]$
$f \rightarrow Flux\ frequency\ in\ Hertz, [Hz].\ Where, \omega = 2 * \pi * f$

After comparing the results of equations (36) and (38), the cross sectional area of the magnetic core was taken to be *16 [cm²]* while designing the model in COMSOL. This defined the height of the core to be 8 [cm] tall and the width to be 2[cm] wide.

Further, for the simulated transformer to have a decent electromagnetic induction between the primary cable and the secondary coil, the cross sectional area of the core can also be evaluated using equation (42). To reach that stage initially the transformer induced voltage in secondary coil has to be formulated using equation (39) similar to

equation (30) which gives the peak secondary voltage. After substituting equations (23) and (24) in equation (40), it is simplified and equation (42) is derived, with which the cross sectional area of the magnetic core is easily calculated to be around *15 [cm²]*.

$$V_{S[MAX]} = N_S * \frac{d\Phi_B}{dt} \tag{39}$$

$$V_{S[MAX]} = \frac{N_S * \mu * A_C * N_P}{l_m} * \frac{d[I_P * \sin(\omega t)]}{dt}$$

$$V_{S[MAX]} = \frac{N_S * \mu * A_C * N_P}{l_m} * I_P * \omega * \cos(\omega t) \tag{40}$$

$$At, \quad Time \rightarrow t = 0, \quad \cos(\omega t) = 1, \quad and \quad \omega = 2\pi f:$$

$$\sqrt{2} * V_{S[RMS]} = \frac{N_P * N_S * \mu * A_C * 2\pi f * I_P}{l_m} \: [V] \tag{41}$$

$$A_C = \frac{\sqrt{2} * V_{S[RMS]} * l_m}{N_P * N_S * \mu * 2\pi f * I_P} = \frac{\sqrt{2} * V_{S[RMS]} * l_m}{2\pi f * \mu_0 * \mu_r * N_P * N_S * I_P} \tag{42}$$

$$A_C = \frac{\sqrt{2} * 230 \: [V] * 0.25133[m]}{2\pi * 6000[Hz] * 4\pi * 10^{-7} \left[\frac{H}{m}\right] * 200 * 1 * 5.75 * 1000[A]} \approx 0.0015[m^2] \approx 15[cm^2]$$

4.1.3. Calculating Number of Secondary Coil Turns and Load Impedance

The transformer model designed for simulation with all the desired parameters, required load impedance attached to the secondary windings (coil) for it to function and give accurate results based on the calculations performed as shown in figure 20. The load impedance (Z_L) value is calculated using equation (43), and solving equations (44) and (45) gives the number of turns (N_S) required in the secondary coil.
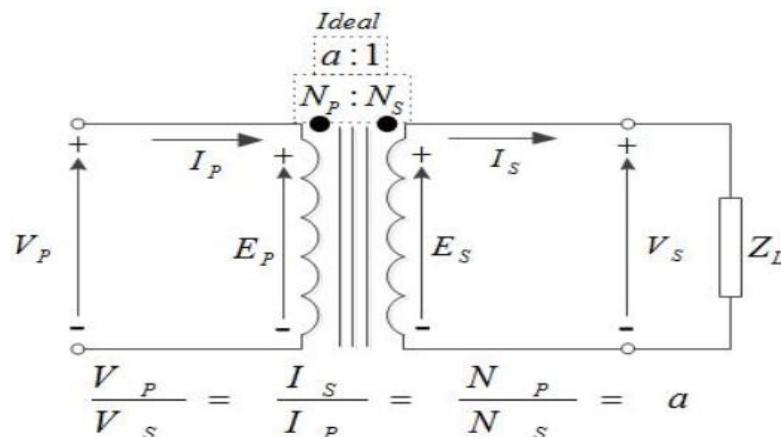
Figure 20: Ideal transformer circuit diagram

$$Z_L = \frac{V_L}{I_L} = \frac{V_S}{I_S} = \frac{230\ [V]}{174\ [A]} \approx 1.32\ [\Omega] \tag{43}$$

$$Coils\ Turn\ Ratio, \qquad a = \frac{I_S}{I_P} = \frac{174\ [A]}{1000\ [A]} = 0.174 = \frac{N_P}{N_S} \tag{44}$$

$$N_S = \frac{1}{0.174} = 5.75 \approx 6\ [Turns] \tag{45}$$

From the above calculations, if the voltage is increased, then the current is decreased by the same factor. The impedance in one circuit is transformed by the *square* of the turn ratio *[a]*. The apparent impedance of the secondary circuit with load *(Z_L)* or the effective input impedance *[Z_{P-eff}]* at the primary terminals can be *referred* to the primary winding circuit as derived in equation (46).

$$Z_{P-eff} = \frac{V_P}{I_P} = a^2 * \frac{V_S}{I_S} = 0.174^2 * Z_L = 0.030276 * 1.32 \approx 40[m\Omega] \tag{46}$$

For example, if an impedance Z_L is attached across the terminals of the secondary coil,

it appears to the primary circuit to have an impedance of $\rightarrow \left(\frac{N_P}{N_S}\right)^2 * Z_L = a^2 * Z_L$

This relationship is reciprocal, so the impedance Z_P of the primary circuit appears to the

secondary as: $\quad \left(\frac{N_S}{N_P}\right)^2 * Z_P = \frac{1}{a^2} * Z_P$

Similarly, $\quad V_P = a * V_S = 0.174 * 230[V] \approx 40\ [V]$

4.1.4. Calculating Resistances of Primary Cable and Secondary Coil

The Electro Motive Force [EMF] in an electric circuit can also be represented as equation (47) where R is the resistance of the conductor (wire) and I is the current flowing through it in the circuit.

$$EMF \rightarrow E\ or\ V = R * I\ [\boldsymbol{V}] \tag{47}$$

$$R = \frac{\rho * l_c}{A_W} = \frac{l_c}{\sigma * A_W}\ [\boldsymbol{\Omega}] \tag{48}$$

Here,
$\rho \rightarrow Resistivity\ of\ the\ Electrical\ Material\ for\ example\ a\ copper\ wire\ or\ cable.$
$\quad Resistivity\ of\ Copper, \qquad \rho_{Cu} = 1.68 * 10^{-8}[\Omega m]$

$A_W \rightarrow Cross\ sectional\ area\ of\ the\ wire.$
$l_c \rightarrow Length\ of\ the\ cable\ or\ wire.$
$\sigma \rightarrow Conductivity\ of\ the\ wire\ or\ cable.$
$\quad Conductivity\ of\ Copper,\ \sigma_{Cu} = 5.96 * 10^{-7} \left[\frac{S}{m}\right]$

Using equation (48), resistance of the primary cable with a radius of 1 [cm] or 0.01 [m] and having a circular length of around 100 [m] is calculated in equation (49).

$$R_P = \frac{1.68 * 10^{-8} * 100}{\pi * (0.01)^2} = 0.00535 \, [\Omega] = 5.35[m\Omega] \tag{49}$$

$$R_P = \frac{1.68 * 10^{-8} * 1.05}{\pi * (0.01)^2} = 56.15 \, [\mu\Omega] \approx 60 \, [\mu\Omega] \tag{50}$$

Similarly, the resistance of the primary cable with a radius of 1 [cm] or 0.01 [m] and having a circular length of 105 [cm] or 1.05 [m] is calculated in equation (50).

To measure the resistance of the secondary coil, which is coiled around a cylindrical-square shaped soft iron core with a height of 8 [cm] and a width of 2 [cm], first the radius of the wire used to make the secondary coil is calculated with equations (51) and (52). Using the number of turns of the secondary coil from equation (45), radius of the primary cable $r_P = 1 \, [cm]$, and applying the principle of power-in is equal to power-out; the number of turns times the cross-sectional area of the secondary coil should be equal to the number of turns times the primary cable cross-sectional area, the values are substituted in equation (51). **[9. 10.]**

$$N_S * A_S = N_P * A_P = 6 * \pi r_S{}^2 = 1 * \pi r_P{}^2 \tag{51}$$

$$r_S = \sqrt{\frac{1}{6}} = 0.40825 \, [cm] \approx 0.41[cm] \tag{52}$$

$$R_S = \frac{\rho * l_c}{A_W} = \frac{\rho * 6 * Perimeter \, of \, the \, coil \, around \, the \, core}{Cross - sectional \, area \, of \, the \, wire} \tag{53}$$

$$R_S = \frac{1.68 * 10^{-8} * 6 * (2 * (0.0841 + 0.0241))}{\pi * (0.0041)^2} \approx 0.41[m\Omega] \tag{54}$$

With the radius of the secondary coil wire known, its diameter is 0.8165 [cm]. To calculate the resistance of the secondary coil (R_S) with 6 turns around the soft iron core which gives the coil a rectangular shape is performed using equations (53) and (54). Upon computing the model simulation the resistances of the primary cable and secondary coil were also measured by the software as displayed in table 3 on the following page. These resistances match quite close to the calculated values in equations (49), (50) and (54); and this is quite promising in stating that the simulated model would give precise results as an actual model if built physically in a laboratory.

Table 3: Cable and Coil Resistances (mf.RCoil_Cable : mf.RCoil_Coil)

Time (µs)	Cable Resistance (DC) [Ω]		Coil Resistance (DC) [Ω]
499.99	Length 100 [m]	0.0053128	3.9280982*E-4
	Length 100 [cm]	6.1612146*E-5	4.0750981*E-4

4.2. COMSOL Multiphysics Simulation Design Parameters

4.2.1. Soft Iron Core B/H Properties

A nonlinear B-H curve that includes saturation effects has been used to simulate the magnetic behaviour of the soft-iron core designed in this model. Hysteresis effects in the core were neglected. Many ferromagnetic materials exhibit nonlinear behaviour, as the magnetization depends nonlinearly on the magnetic fields. These materials also exhibit *hysteresis*, a dependence of the applied magnetic field on magnetization. Modelling hysteresis behaviour is computationally demanding and difficult. The nonlinear magnetic materials available in the AC/DC Module of COMSOL Multiphysics does not include the full hysteresis loop, but instead the average BH curve that incorporates magnetic saturation effects in the first quadrant as shown in figure 21.
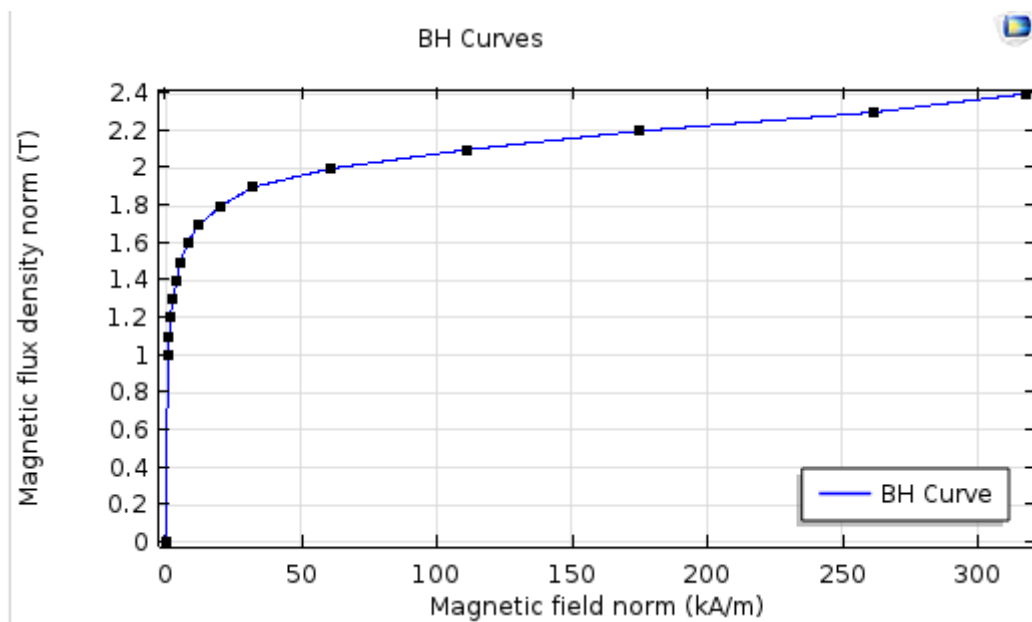
Figure 21: B/H Graph from COMSOL of Soft Iron Core (without losses).

An average value is reasonably representative of the magnetic material properties, and the resulting curve is known as the *normal magnetisation characteristic curve.* These magnetic saturation curves can be used directly in the stationary and time-dependent studies to compute electro-magnetic models built for simulation. **[11, 1.]**

4.2.2. Device parameters

External electric circuit elements were added to the primary and the secondary side of the contactless power transfer model simulation. Electrical nodes were assigned in a sequence to all the elements so that they connect appropriately and behave accordingly on computing the model, as shown in figure 22. Node 0 (zero) is the common node and always acts as a ground in both the parallel circuits. Between node 1 (one) and node 0 (zero), assigned to be positive and negative nodes respectively, the voltage source was placed. Alternatively between node 0 and 1, the primary cable was placed completing the circuit. Similarly between node 2 (two) and node 0 (zero), the secondary coil is placed. Here the magnetic core is not connected to any nodes since it becomes active when there is current flowing through the primary cable. The cable's magnetic field is magnified by the core and influences the secondary coil, making it come alive which could easily be monitored on generating the results.
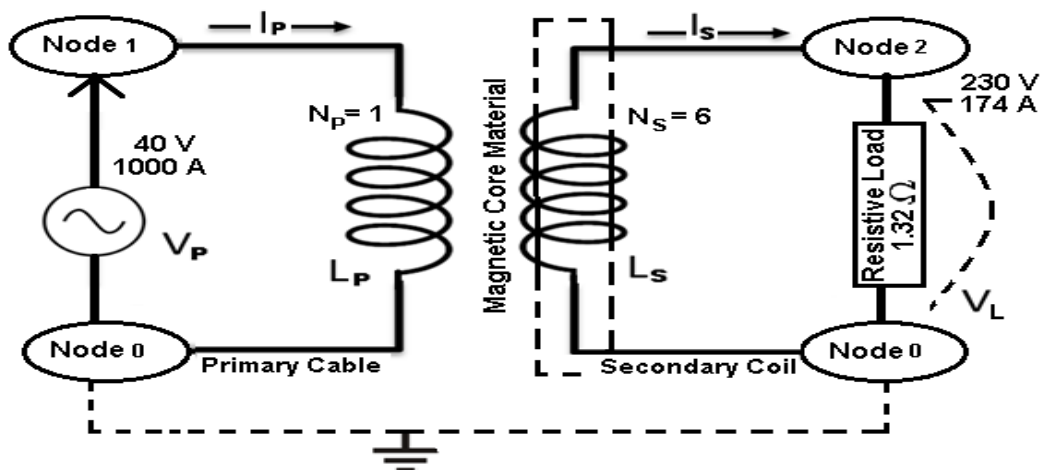
Figure 22: Electric Circuit Schematic of the model built for simulation.

The power supply required on the primary side was already known and the parameters shown in figure 23 were set for the sine source between nodes one and zero.

Figure 23: Setting source voltage and frequency of primary cable.

4.2.3. Time Dependent Solver

The syntax of time range 0:8.3333:500, as shown in figure 24, represents a vector of times starting at 0 with steps of 8.3333 up to 500 [μs]. It was calculated using the frequency and time relationship which are inversely proportional to each other. Hence, one time period of 6 [kHz] is 166.67 [μs]. Each time period are divided into 20 steps of 8.3333 [μs]. Finally three complete time periods are achieved after 500 [μs].
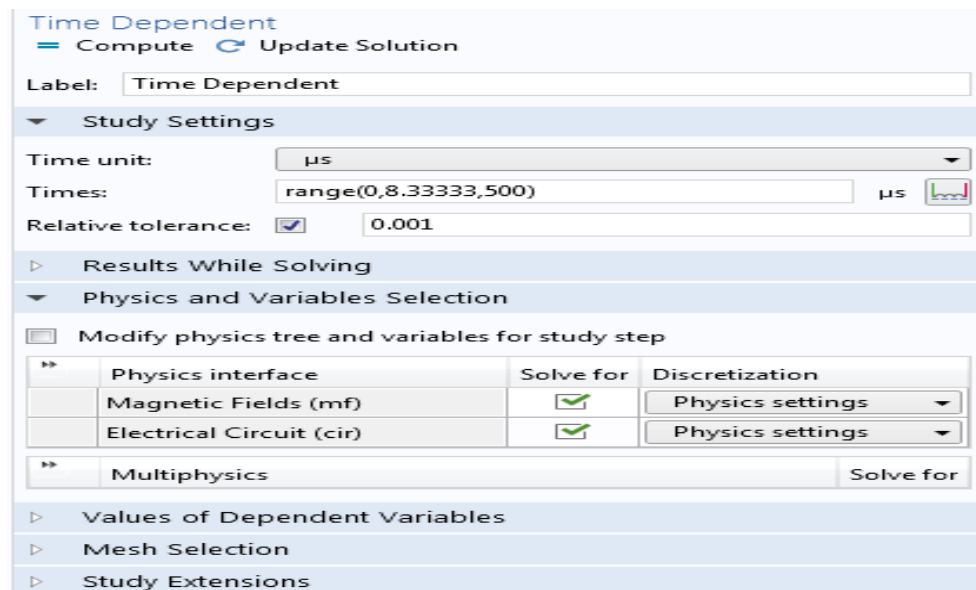
Figure 24: Time Dependent Solver settings window displayed in software.

For accurate results and a smooth computation of the model, the default absolute and relative tolerance parameters for the time-dependent solver which controls the error in each integration step, can be further reduced from their default values respectively. Roughly stated, relative tolerance controls the accuracy of time dependent solver which is non-linear in nature. As shown in figure 24, the relative tolerance before computing the models has been reduced from the default value of 0.01 to 0.001. The lower the tolerance value, shorter is the time-steps taken by the solver while computing the model, hence all the model structures computed, namely A, B and C, took around 30 minutes to complete the computation process before generating any results. The tolerance factor as shown in figure 25 has also been changed from its default value of 1. Figure 25 is taken from the model builder menu appearing on the left side of the COMSOL software main page. Further selections can be seen in the sub-menus where a fully coupled nonlinearity ramping techniques were selected. A fully coupled approach has been used to solve this multi-physics nonlinear time dependent problem, which also uses the same damped algorithm used for solving a single physics nonlinear problem. The fully coupled solver started with an initial guess and

then applied the Jacobian iterations until the solution got converged as seen in figure 26, though it follows a monotonic pattern. The stability of the nonlinear process is maintained by updating the Jacobian after each iteration is computed, whose maximum limit is predefined otherwise it is controlled by the tolerance factor.
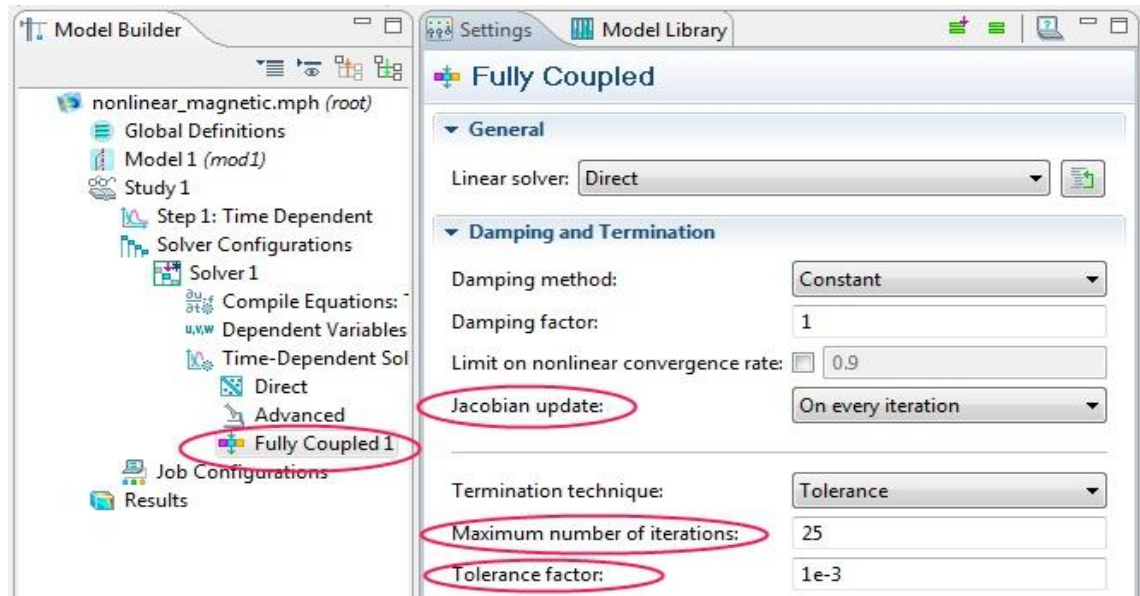

Figure 25: Time dependent solver settings.

Figure 26 shows the time dependent solver graph generated on computing the model illustrating the time taken to perform all the mathematical calculations and iterations in the background while formulating all the results of the model being simulated.
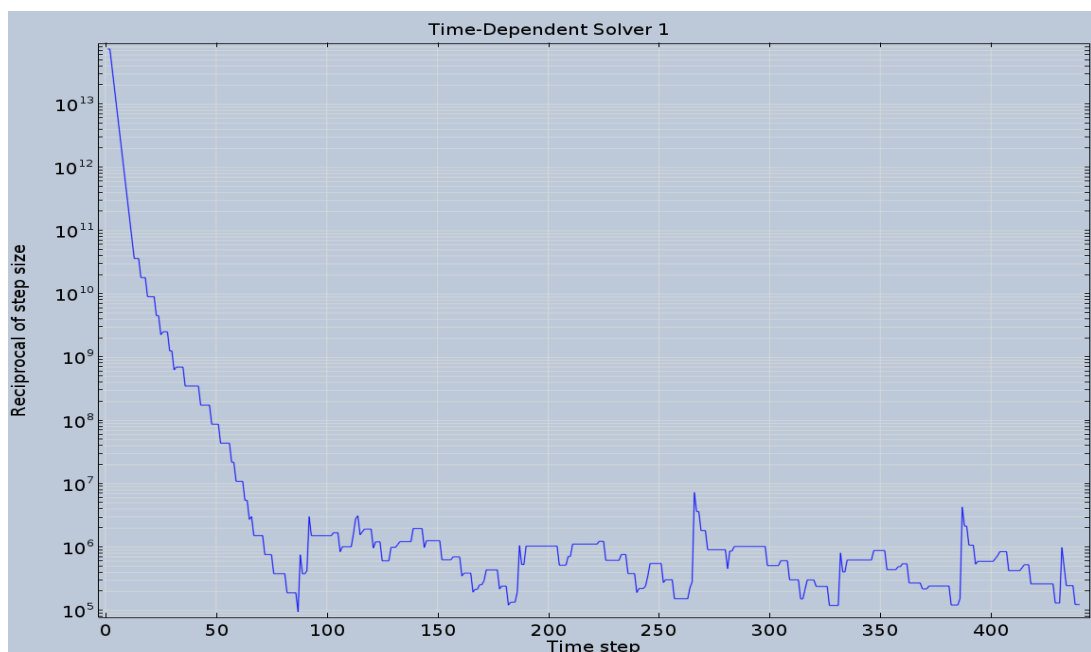
Figure 26: Time dependent solver graph

Figure 27 illustrates the convergence plot that is generated when the model is computed in any of the study modes. The plot in figure 27 shows the decrease in error when each physics is being solved. Iterative methods compute the solution gradually where the error estimate can be observed in the solution which decreases with increase in number of iterations. Normally the two segregated steps should converge at the end of the final iteration number. This reflects that more iteration may be required to eliminate the error in the model built either due to the co-ordination of various geometries or when the model is meshed together before being computed. This could be due to the fact that some of the geometry shapes are relatively smaller in size with respect to its domain and hence the joints where the different meshes merge find it hard to compute the results. Strong nonlinearities could also be a factor for non-convergence of the plot.
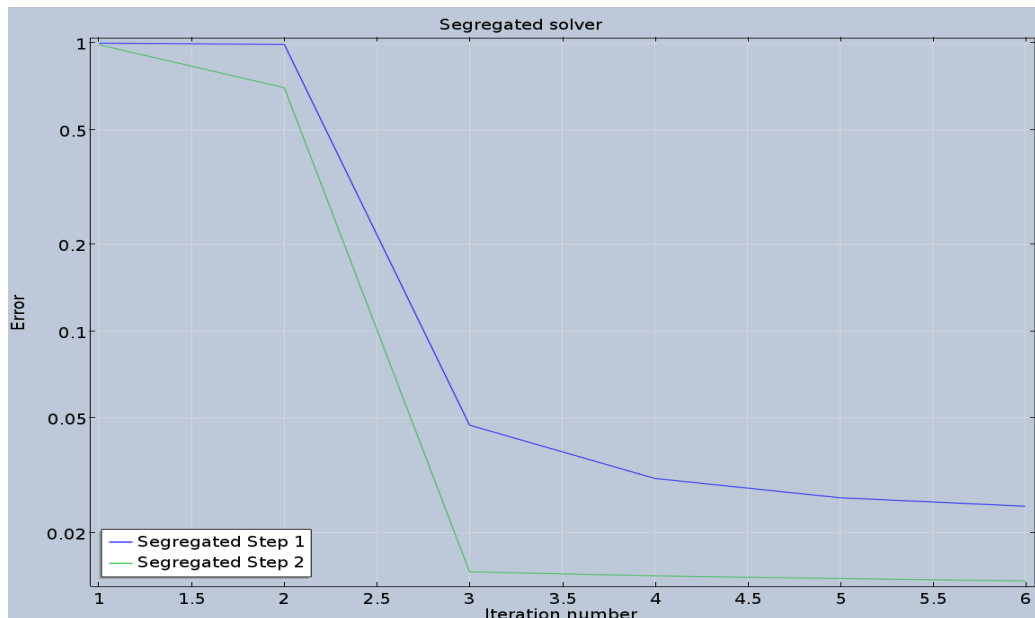
Figure 27: Segregated solver graph

5.   Discussion

In general, two wireless power transfer 3D transformer models were built for simulation purpose with different lengths of primary cable, being 100 [m] and 100[cm] respectively. And then the results were analysed to compare the similarities of the power output in both the cases. After constructing the geometrical structure of the model with all its elements, it had to be enclosed in an air domain having a cylindrical or block shaped boundary for generating accurate results. It is illustrated in figure 28.

Geometrical Structure of the model built for FEM Simulation

Primary Cable

Soft Iron Core
(Without Losses)

Secondary Coil

Block Outline of the Air Region
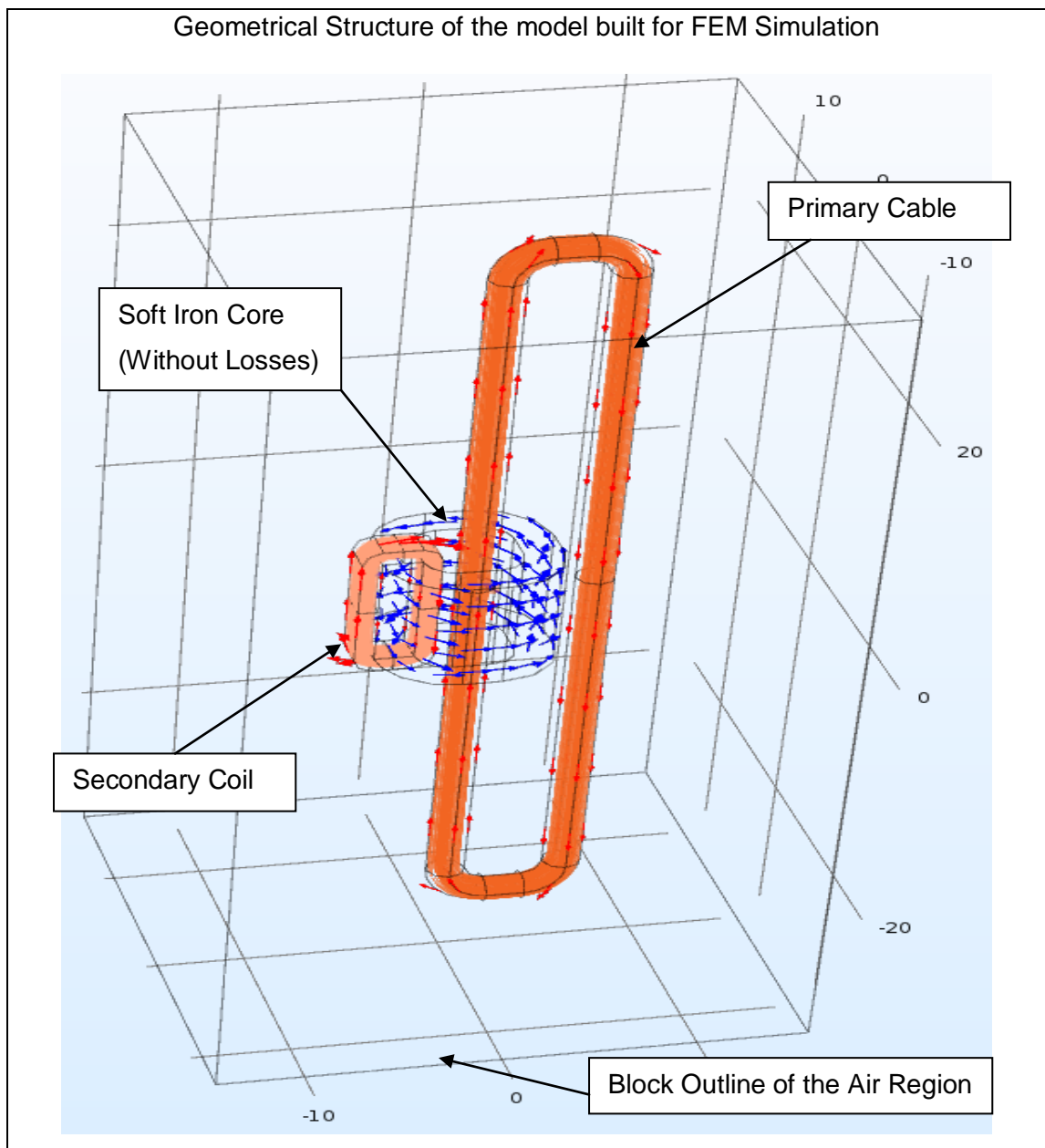
Figure 28: Model structure used for simulation. Red arrows depict the current flow in the primary cable and secondary coil. Blue arrows depict the magnetic field generated in the soft iron core due to electromagnetic induction.

The 3D geometries were created by initially modelling a 2D cross section and then building 3D objects using extrude and revolve operations. In COMSOL Multiphysics 2D cross sections are created in a local 2D coordinate system known as a work plane, which can be positioned anywhere in the 3D space. A 2D plane defines a work plane parallel to the xy-plane, yz-plane, or zx-plane, and the z-axis direction of the work plane is parallel to z-axis direction, x-axis direction, or y-axis direction of the 3D geometry model, respectively.

Meshing of the geometrical structure is required before the model can be computed as shown in figure 29. A mesh is a partition of the geometry model into small units of simple shapes. In 3D the mesh generator partitions the sub-domains into tetrahedral, hexahedral, or prism mesh elements whose faces, edges, and corners are called mesh faces, mesh edges, and mesh vertices, respectively. The boundaries in the geometry are partitioned into triangular or quadrilateral boundary elements. The geometry edges are partitioned into edge elements. Isolated geometry vertices become mesh vertices. The value in the Maximum element size edit field specifies the maximum allowed element size, which by default is 1/10th of the maximum distance in the geometry. This parameter is optional however is quite important to select the correct size from coarse to fine which either decreases or increases the computing time.

Free Tetrahedral mesh is used everywhere in the model.
Normal mesh size is selected for the Core, Primary Cable and Secondary Coil.

Primary Cable

Secondary Coil

Magnetic Core

Block - Air region
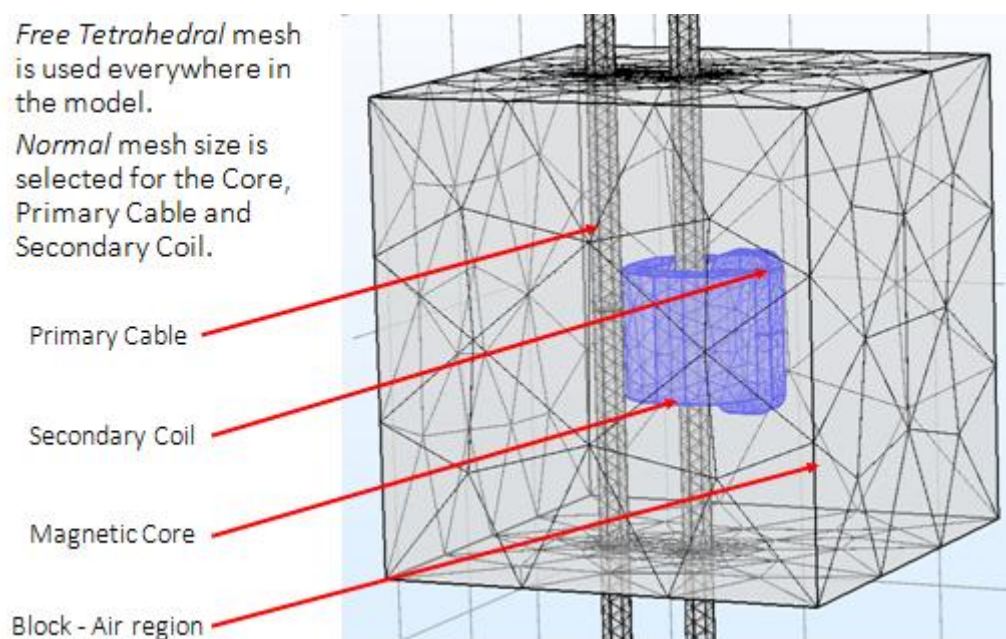
Figure 29: Mesh model of the structure built for simulation. The air block is constructed enclosing the core area only and its mesh size is extra coarse.

Altogether there were over ten models built for simulation to study this project topic and some of them were basically used for learning COMSOL Multiphysics software. After deriving some accurate results based on the mathematical calculations three model structures were selected to analyse the results and reach a conclusion. A fourth model was also computed but it took a considerable amount of time to generate any results. Also, initially there were a few errors in the model design which failed to find a solution on computing stating 'Returned solution is not converged'. Anyhow after following some trial and error techniques learned from COMSOL blogs, accurate results were generated in a good time frame.

5.1.   Model Structure A

In the first simulation model the length of primary cable in a loop is 105 [cm] and the whole geometrical structure is enclosed inside the air block of cylindrical shaped domain. The following are the graphical results created by the software after computing the simulation model. Figure 30 illustrates the magnetic flux density recorded at various locations in the circuitry and the intensity could be compared with the colour label on the side with markings in Tesla. This is the figure generated by default since the model study was performed in the magnetic field domain. Thing to note here is that the intensity of the colour does not show the maximum flux density achieved when current flows through the circuit. Since the model was simulated for three complete time periods, figure 30 image could be of any time interval from start to finish. Figure 31 illustrates the flow of the current in primary cable and secondary coil with red coloured arrows, and the magnetic field in the core with blue coloured arrows.
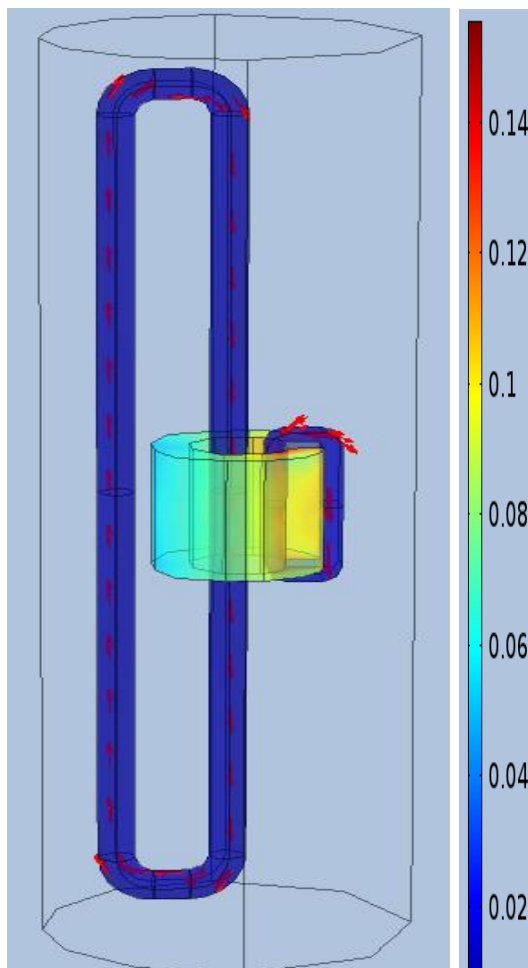
Figure 30: The Magnetic Flux Density   Figure 31: Current flow and magnetic field
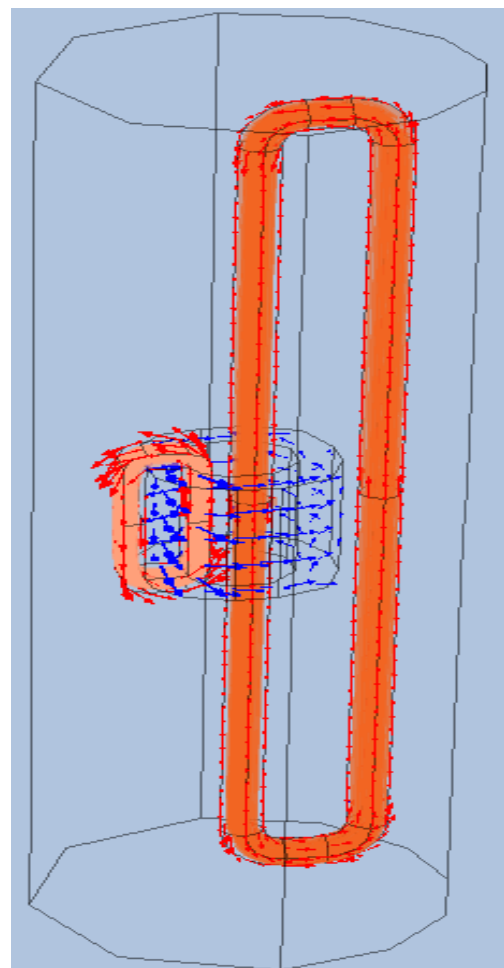
The actual hysterical graph of the magnetic flux fluctuating inside the core could be observed in figure 32. It is quite interesting to observe the change in magnetic flux with

respect to the change in the alternating current in the primary cable as shown in figure 35 below. Majority of the graphs and figures were retrieved after the computation of the model, which were generated after selecting the specific desired outcomes under the Results menu. There were two study domains selected before simulating the model, the magnetic field and electric current respectively; and they both generate graphs with respect to the properties associated with them.
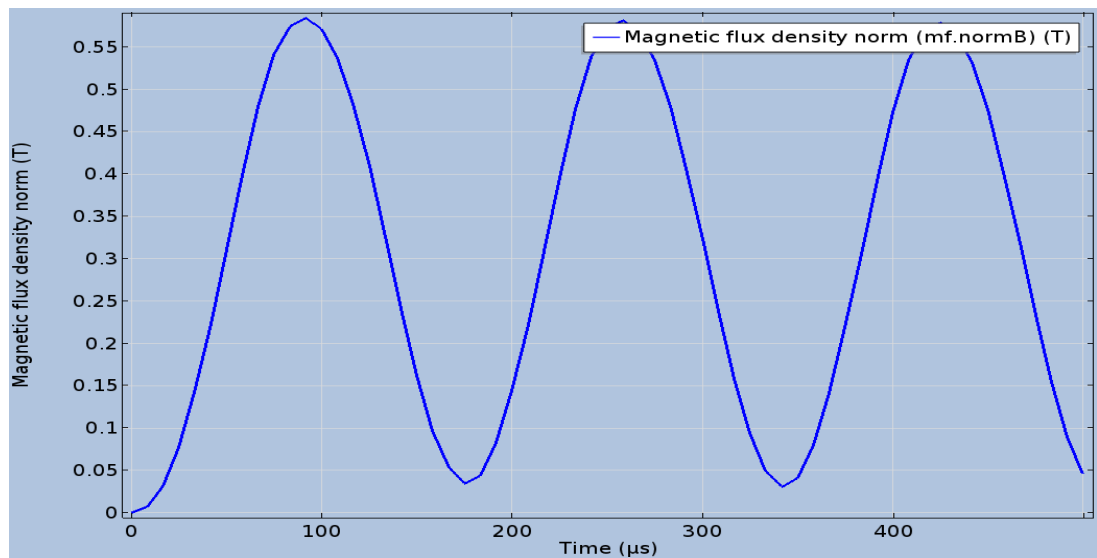
Figure 32: Magnetic Flux Density normal in the Magnetic Field domain
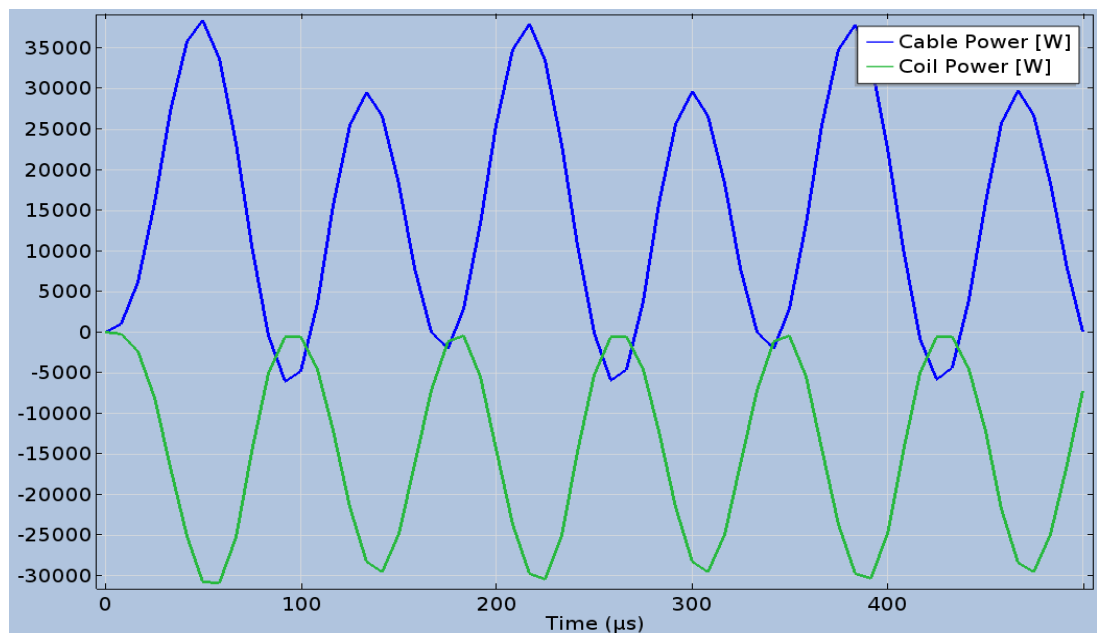
Figure 33: Comparing Power In and Power Out $\rightarrow$ 100 [cm] Full Block

Figure 33 clearly shows the power input with respect to the power output and are almost equal but opposite in phase. Similarly, the voltages shown in figure 34 are

opposite in phase but the currents are in the same phase, which is how a transformer should behave ideally as shown in figure 35.
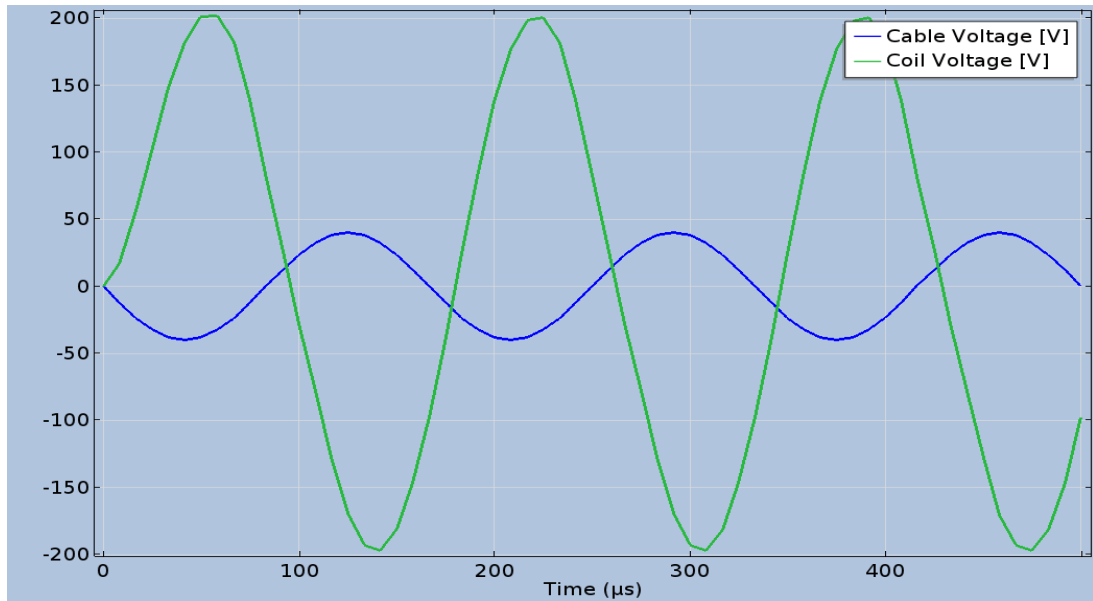
Figure 34: Comparing Voltages in Primary Cable and Secondary Coil
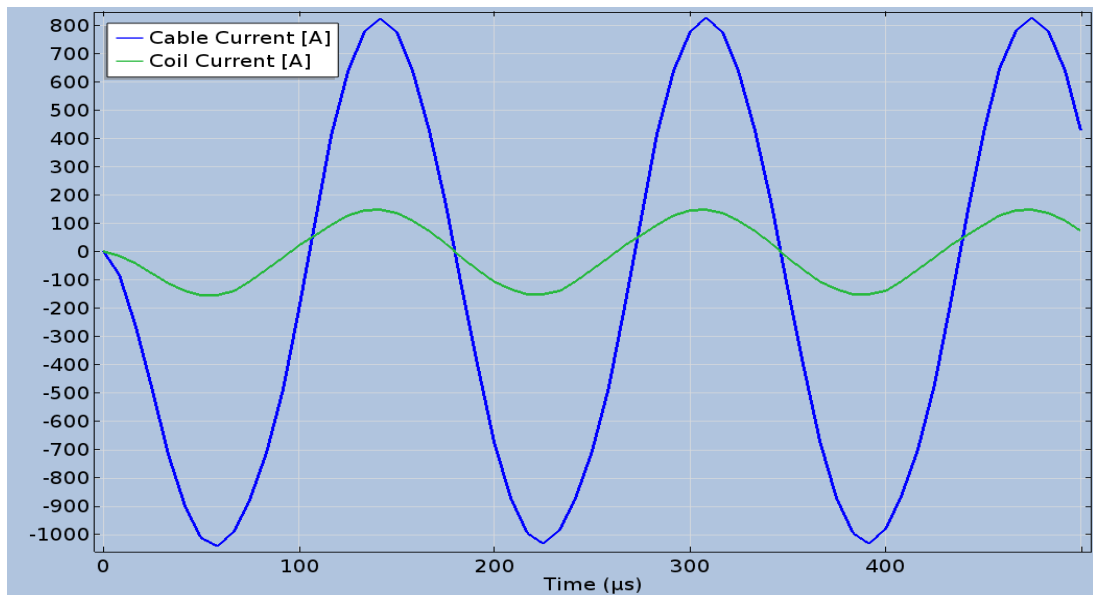
Figure 35: Comparing Current in Primary Cable and Secondary Coil

On the following page figure 36 displays the direction of the windings of primary cable and the secondary coil in the circuit with a bold red arrow. Similarly figure 37 illustrates the mesh structure created before the model is computed. It clearly displays the whole model structure with primary cable of loop length 105 [cm] and all other components, inside the air block region completely, which is cylindrical in shape. This air block region could be of rectangular box shape, without affecting the computation results.
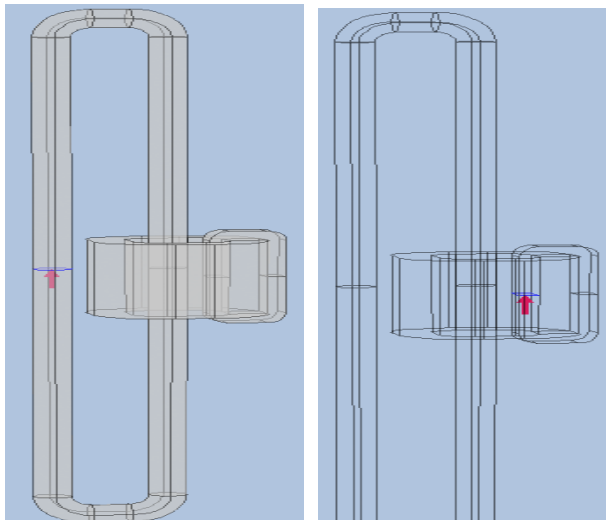
Figure 36: Winding directions
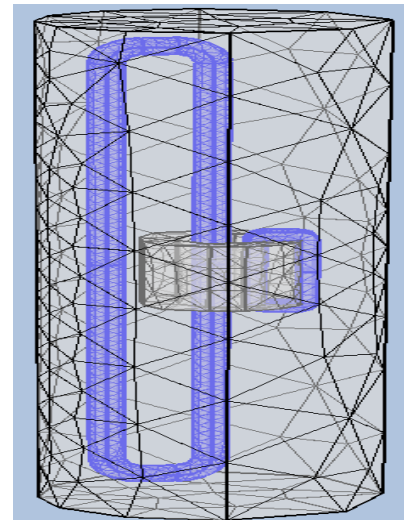
Figure 37: Mesh structure

5.2.   Model Structure B

In the second simulation model only a limited section of the whole circuit was contained inside the air block region and the electro-magnetic effects were computed. The length of the primary cable loop is still around 105 [cm] and only the core area geometry was enclosed inside the air block domain. In figure 38 and 39 the flow of the currents in both the cable and the coil is shown with red arrows. Figure 38 also shows the intensity of the magnetic flux in the circuitry at a specific time interval alongwith the colour label in [T]. The blue cones in figure 39 shows the concentration of the magnetic field in the core where the secondary coil is wounded around it.
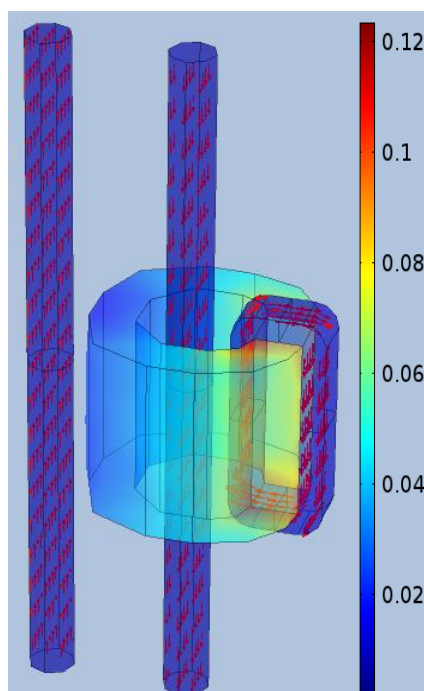
Figure 38: Magnetic Flux
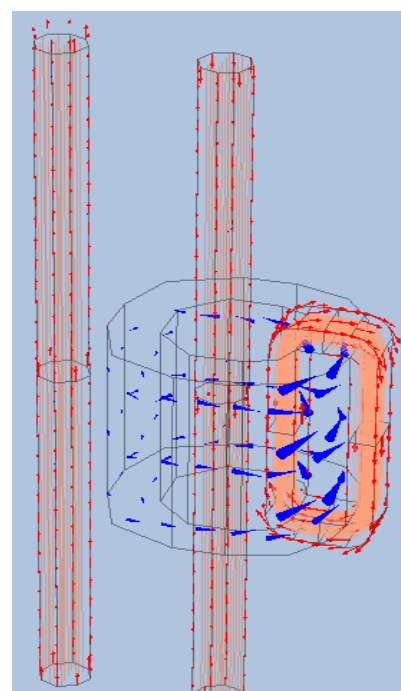
Figure 39 current and magnetic flow
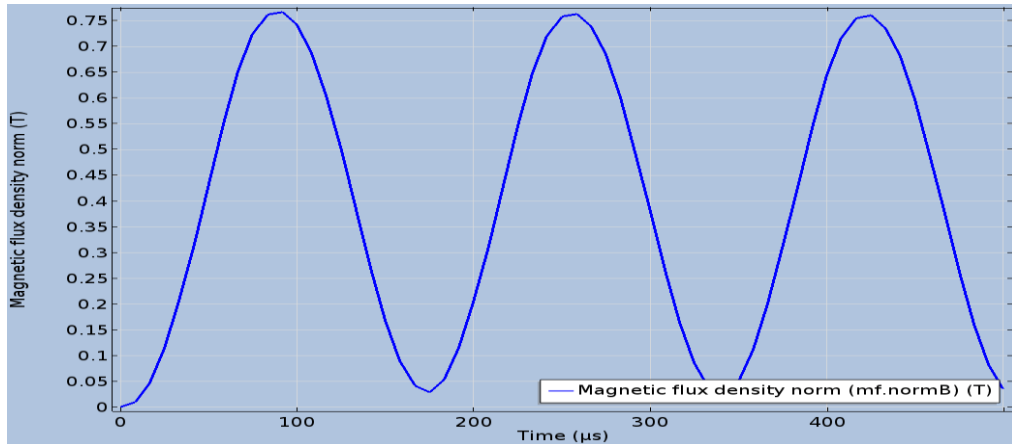
Figure 40: Magnetic Flux Density normal in the magnetic field study domain.

Figure 40 shows the magnetic field alternating with respect to the current flow and it can be observed in figure 41 the magnetic flux saturation due to hysteresis in the core.
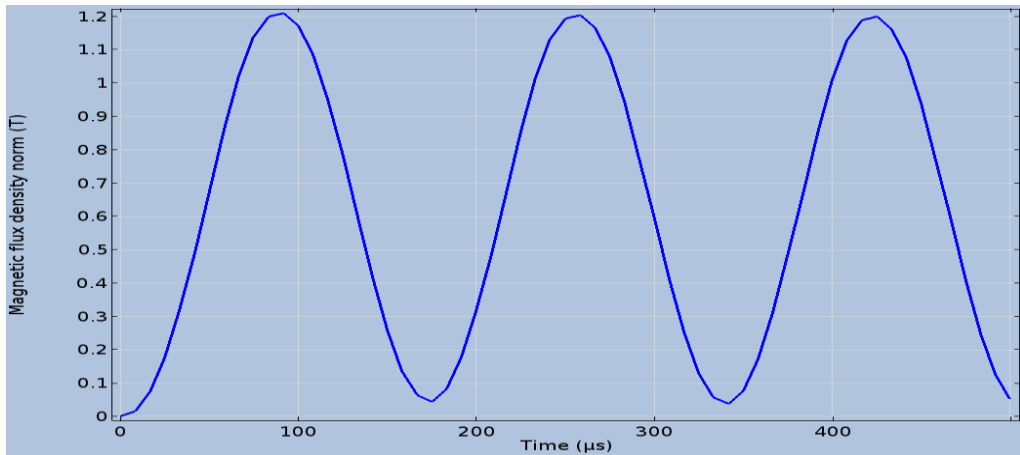

Figure 41: Saturation of the magnetic flux density in the core.

The following graph in figure 42 shows the power levels produced both in the primary cable and secondary coil with respect to the time periods. It is almost close to 40 [kV] as per the calculations performed previously.
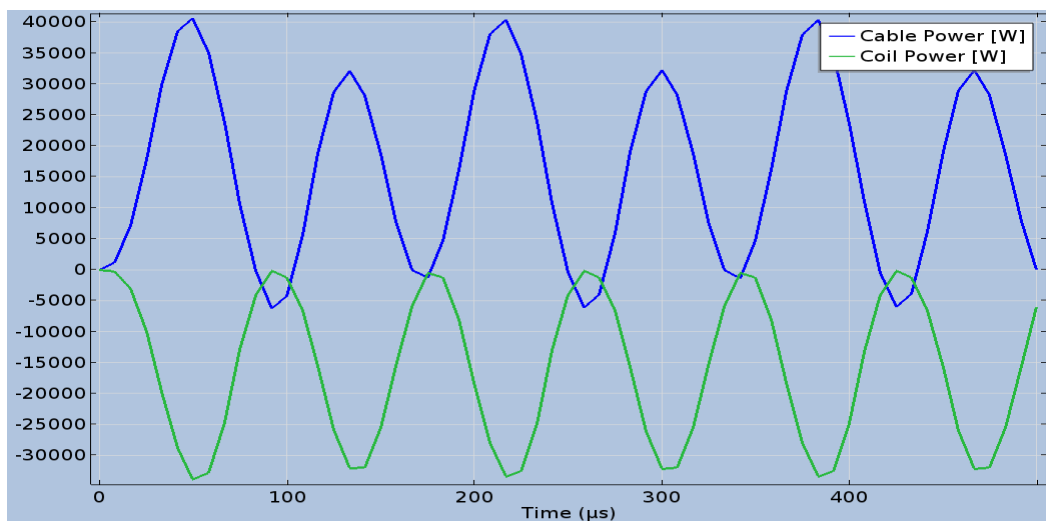
Figure 42: Comparing Power In and Power Out → 100 [cm] Core Block only

The results obtained from this simulation in which only the area around the core was encapsulated inside the air block, almost precisely match with the calculated mathematical model. Figure 43 and 44 clearly shows the voltages and currents produced respectively by the circuitry. However, there is a noticeable phase shift which could be due to not taking into account the resonant coupling between the primary and the secondary circuits; and various other factors effecting transformer efficiency.
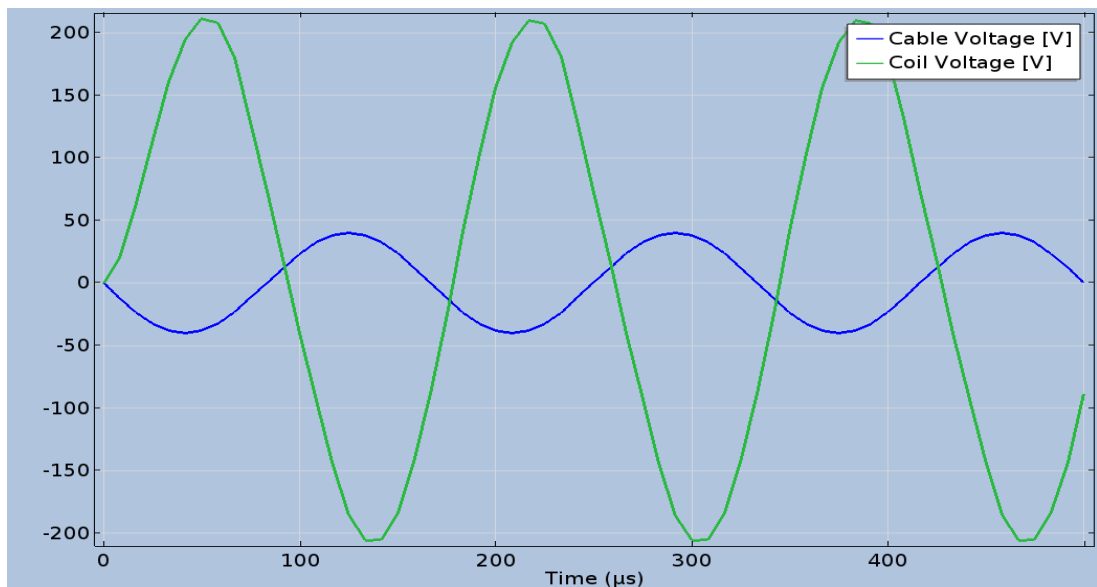
Figure 43: Comparing Voltages in Primary Cable and Secondary Coil
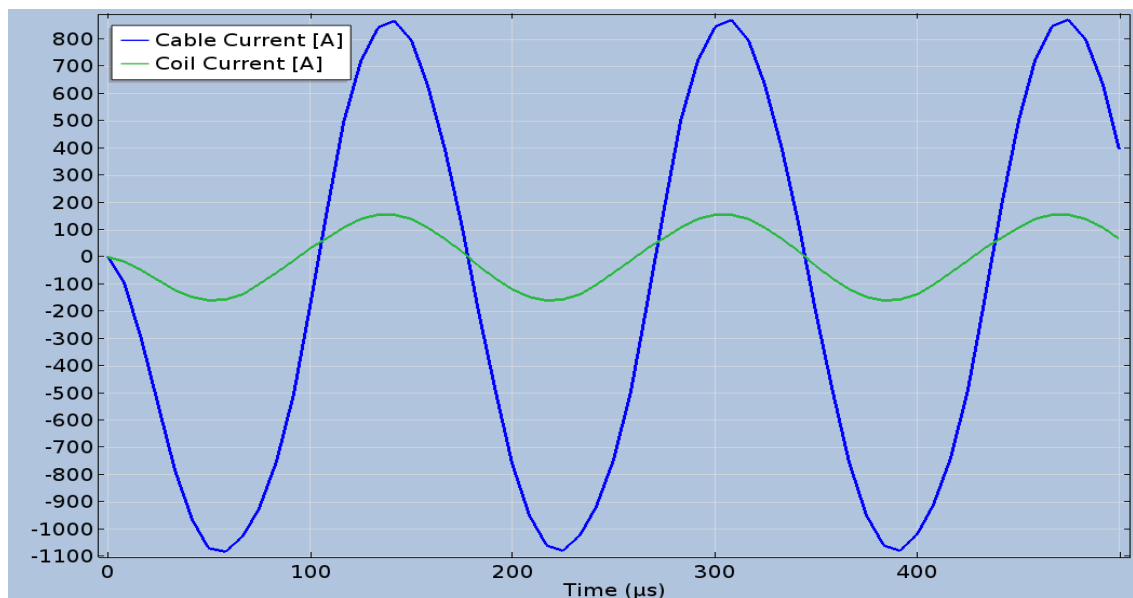
Figure 44: Comparing Currents in Primary Cable and Secondary Coil

In figure 45, the direction of the windings in primary and secondary are indicated with red bold arrows. Upon simulation it did not have a significant effect on the process of power transfer when source voltage was applied. To conduct this experiment

practically, winding of the coils would have an effect on the behaviour of the transformer. Figure 46 illustrates the mesh structure of the model used for simulation.
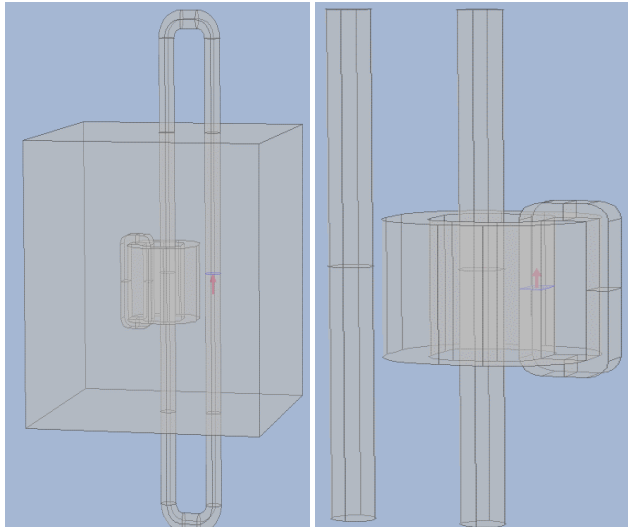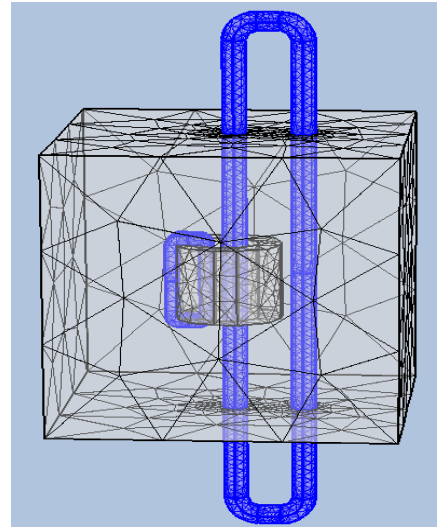

Figure 45: Winding directions   Figure 46: Mesh structure

5.3.   Model Structure C

In the third simulation model the length of the primary cable loop is around 100 metres, and only the core area geometry is enclosed inside the air block domain.
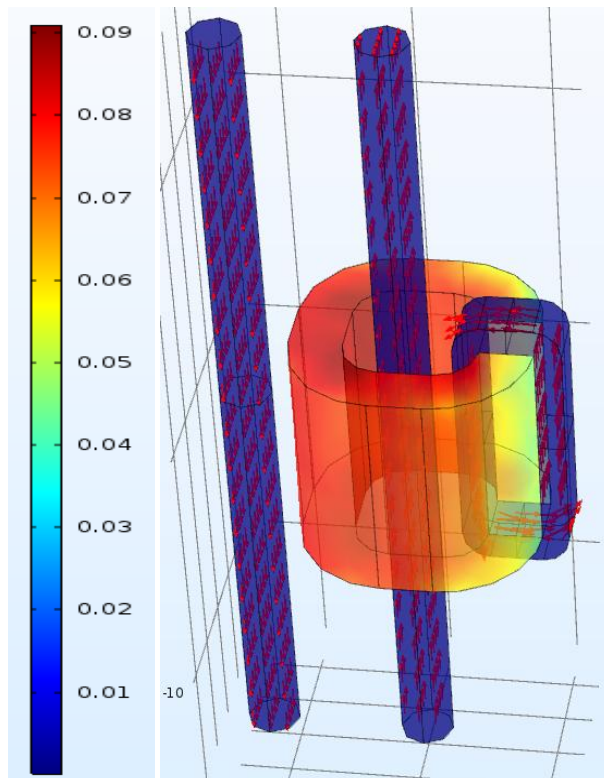

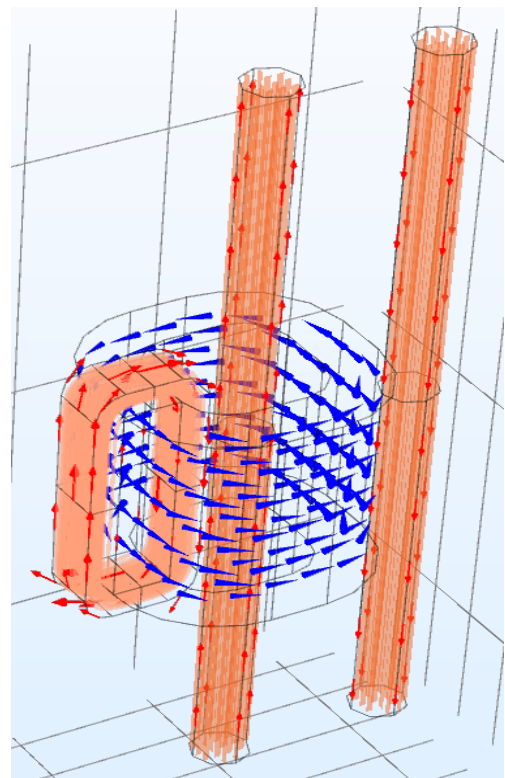Figure 47: Magnetic Flux Density in Tesla [T]   Figure 48: Coil and magnetic flow

The electromagnetic effects are clearly displayed in figure 47 with the flow of the current density in both the primary cable and secondary coil. Figure 48 clearly shows the direction of the current flow and equally distributed magnetic field in the core. The magnetic flux density graph in figure 49 is most probably affected by the length of the primary cable and is not as strong as seen in the Tesla readings when compared with the previous models A and B.
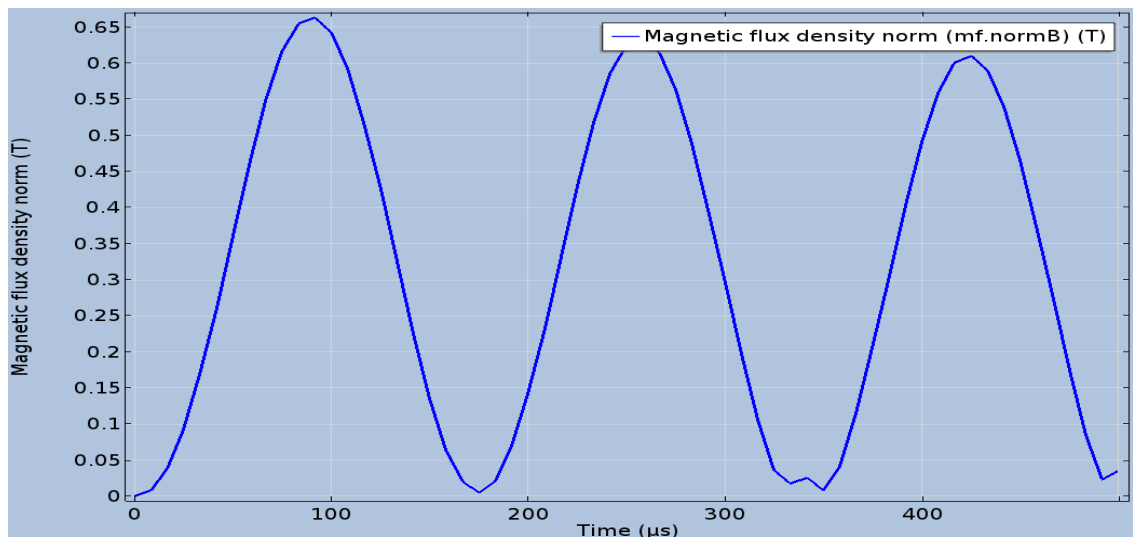

Figure 49: Magnetic Flux Density normal in the magnetic field domain

The power rating is reduced as shown in figure 50 due to the length of the primary cable which increases its resistance. Anyhow there is still a high power transfer taking place between the primary and the secondary circuits. The reason for the power output to be less than the input power in all the cases could be due to the number of turns in the secondary coil or materialistic properties of the conductors.
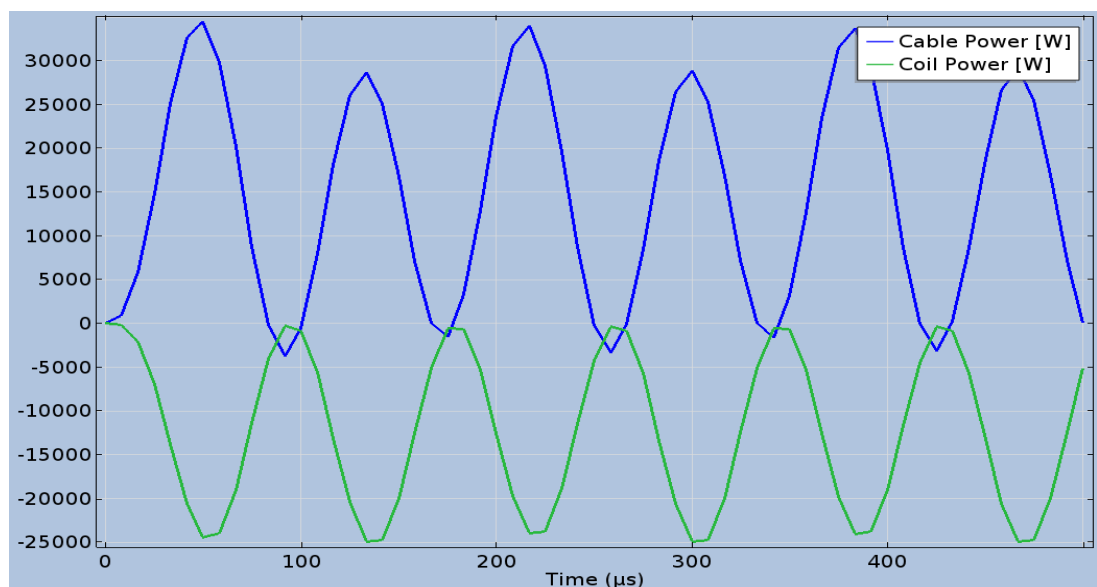

Figure 50: Comparing Power In and Power Out $\rightarrow$ 100 [m] Core Block only

It is quite absurd to clearly observe the phase shift between the voltages in figure 51 whereas the currents in figure 52 seem to be exactly in phase. The voltages and currents values are not at par with the calculated values due to non-resonance. Figure 53 and 54 are self explanatory after reading about previous model simulations.
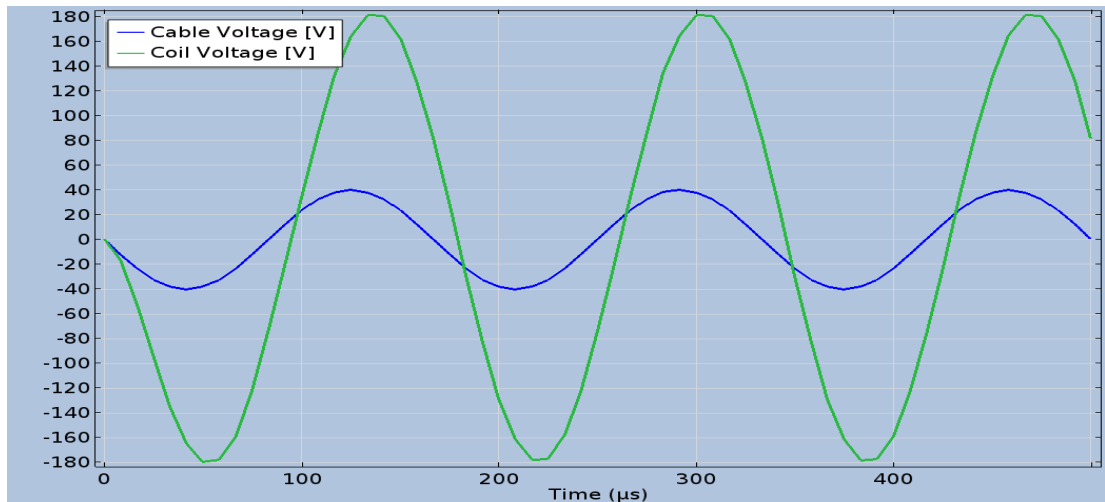

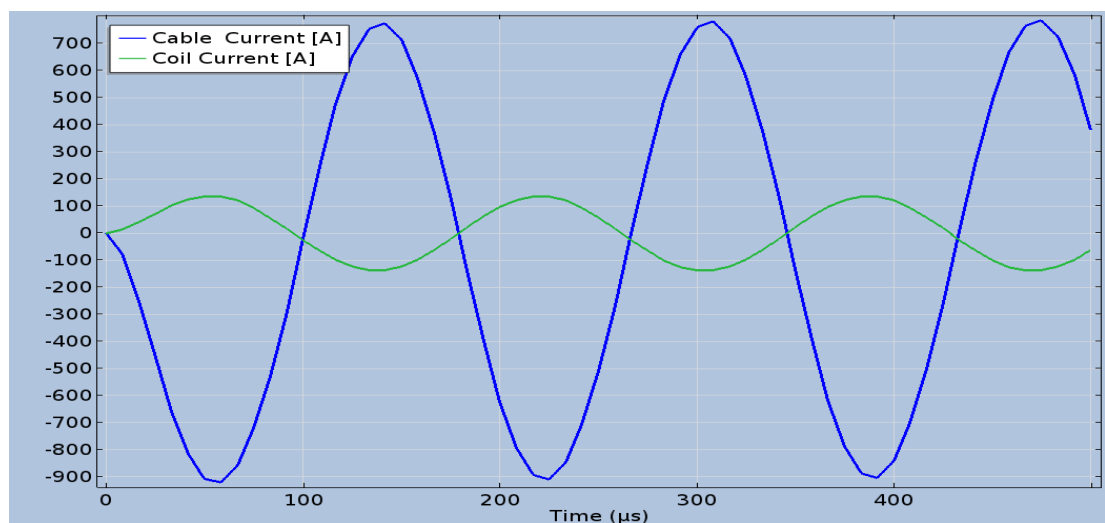Figure 51: Comparing Voltages in Primary Cable and Secondary Coil

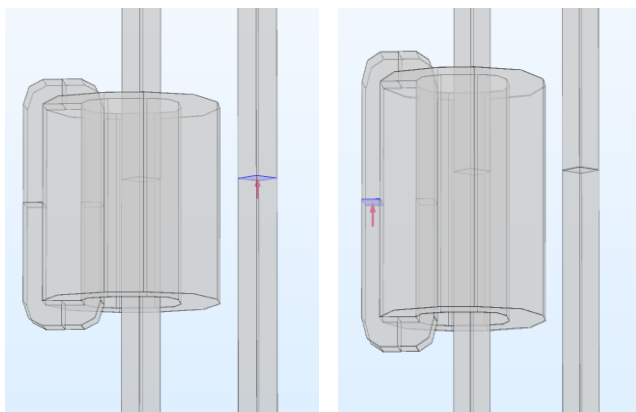Figure 52: Comparing Currents in Primary Cable and Secondary Coil

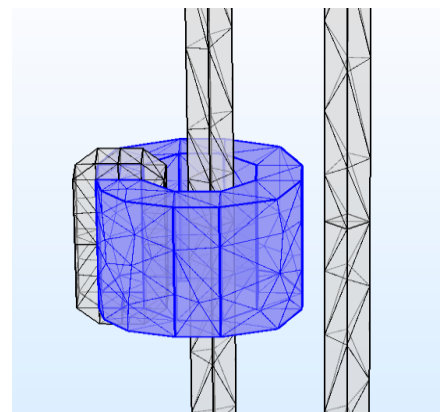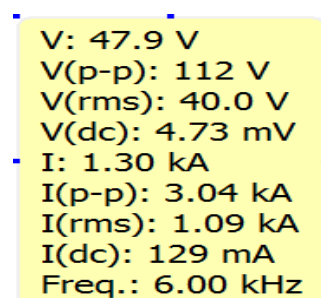Figure 53: Direction of the windings   Figure 54: Mesh structure

6. Conclusion

The goal of the project was to build a high power wireless battery charger system, but after analysing the requirements of the client and the user application area, it was decided to construct a more efficient system which would benefit by reducing the weight where this approach was meant to be applied. However, it was a different concept introduced to the client which they did not anticipate. A physical working model was hard to construct in the institution's laboratory due to the use of a high voltage and current system for which there was a constant requirement of an invigilator.
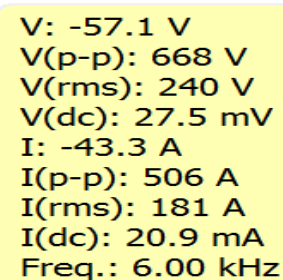
COMSOL Multi-Physics software has been convenient for electro-magnetic simulation, being both insightful and straightforward to build models for generating accurate results. It did take some time to understand its correct usage with all the available tutorials provided by COMSOL. In the final simulation model where the length of the primary cable loop is of around 100 metres, the complete geometry was enclosed inside the air block domain. On visualisation it just looked like a thin long strip, hence no image has been printed because it was hard to see where the core block is in the picture. On building the mesh it was too coarse to resolve steep gradient in the formation. Upon computing the model it was taking well over an hour to solve the model but that too without any meaningful results. The time dependent solver was having trouble converging which might be due to strong nonlinearities. Further if the problem is not well-conditioned then the convergence of the iterative steps is very slow. Also the oscillatory behaviour of the iterative solver indicates that the problem is not properly set-up or the model problem is not adequately constrained.

National Instruments Multisim software was also used for simulating a simple transformer circuit in which probes were attached to the input and output circuit and the results were compared as shown in figures 55 and 56.

V: 47.9 V
V(p-p): 112 V
V(rms): 40.0 V
V(dc): 4.73 mV
I: 1.30 kA
I(p-p): 3.04 kA
I(rms): 1.09 kA
I(dc): 129 mA
Freq.: 6.00 kHz

V: -57.1 V
V(p-p): 668 V
V(rms): 240 V
V(dc): 27.5 mV
I: -43.3 A
I(p-p): 506 A
I(rms): 181 A
I(dc): 20.9 mA
Freq.: 6.00 kHz

Figure 55: Input Probe Readings   Figure 56: Output Probe Readings

In Multisim simulation the resistances of the primary cable and secondary coil was not taken into account and also there was no resonant coupling involved, similarly in COMSOL simulations. It would have had been a more complex circuit if other capacitive or inductive elements were to be added to the circuitry, leading to more mathematical calculation as shown in appendix 2. Overall the models behaved as anticipated referring to the mathematical model, though not exactly, which could be due to the proximity between the loops of the primary cable and secondary coil

There is always a room for improvement by changing the frequency which would further alter the shape and size of the core. Another observation made was whether the direction of the secondary coil winding determines the direction of the current flowing through it. A soft iron core without losses was used in all the simulation models and it was stated to be annealed by default, so it was inconclusive to state the behaviour of a solid iron core. The role of the air block was simply to account for the radiating power of the electric and magnetic fields flowing through the circuit. The model simulation would not have produced any meaningful results if no air block was used to contain all the desired components of the circuit, which are namely the primary cable, secondary coil and the magnetic core. The air block also accounts for the electromagnetic power being radiated outward, the infinite domain outside the block containing the model structure. In the simulation model with 100 [m] primary cable loop (single turn), it was hard to generate optimum results with the whole cable inside the air block, hence could not conclude upon the reliability of the simulation in this case. It could also be advantageous to refine the mesh to solve the multi-physics problems which require different iterative solver settings. Though COMSOL provides built-in default solver settings for all predefined physics interfaces but where to alter the convergence tolerance to provide desired results require more experience working with this software. Further studies in this field are highly recommended to improve the working principles of the wireless power transfer models being simulated using COMSOL Multiphysics.

References

1. Renzi E. Transformer Calculations [online]. Education notes. Florida, USA: Nova Southeastern University; April 2011.
    http://edrenzi.com/Code/Trans (1p).pdf. Accessed 13 April 2017.

2. Devasane M. Single Phase Transformer [online]. GATE EE, January 2017.
    https://gradeup.co/single-phase-transformer-i-9231e297-b2db-11e5-ac47-a72a48007e8a. Accessed 15 April 2017.

3. Erickson R. and Maksimovic D. Fundamentals of Power Electronics, Second edition, Chapter 13 and 15. University of Colorado, Boulder, CO: Kluwer Academic; 2004.
    Erickson R. Introduction to Power Electronics [online]. Lecture Slides, November 2013.
    http://ecee.colorado.edu/~ecen5797/course_material/Ch13slides.pdf
    Accessed 20 April 2017.

4. Williams A. Fundamentals of Magnetic Designs, Inductors and Transformers [Online]. Long Island, USA: Telebyte Incorporation; 15 September 2011.
     https://www.ieee.li/pdf/introduction_to_power_electronics/chapter_12.pdf.
    Accessed 24 April 2017.

5. Article, Winding Configurations, Chapter 9 [online].
    https://www.allaboutcircuits.com/textbook/alternating-current/chpt-9/winding-configurations/ Accessed 24 April 2017.

6. Current Transformer Basics and Transformer Theory [online]. Word-Press; 2013.
    (a) http://www.electronics-tutorials.ws/transformer/transformer-basics.html.
    (b) http://www.electronics-tutorials.ws/transformer/current-transformer.html.
    Accessed 12 April 2017.

7. COMSOL Multiphysics Simulation Software - Platform for Physics-Based Modelling, Electromagnetics Software - Computational Electromagnetic Modeling [online].
    (a) https://www.comsol.com/model/download/264181/models.acdc.ecore_transformer.pdf
    (b) https://www.comsol.com/comsol-multiphysics#overview.
    (c) https://www.comsol.com/acdc-module. Accessed 20 February 2017.

8. Edwards J. Course in Electro-mechanics, Year1 [online]. Course note. Department of Engineering and Design, University of Sussex; 2004.
    http://www.infolytica.com/en/products/trial/docs/Year1%20Document.pdf or
    http://purco.qc.ca/ftp/Learning%20Electronics/General/CourseDocument-2004.pdf.
    Accessed 25 April 2017.

9. Dekker M. Current Transformer Design [online]. Academic Course notes. Charlotte, United States of America: University of North Carolina; 2004.
    https://coefs.uncc.edu/mnoras/files/2013/03/Transformer-and-Inductor-Design-Handbook_Chapter_16.pdf Accessed 18 April 2017.

10. Serway R. and Vuille C. College Physics, Tenth Edition, Chapter 21. United Kingdom: Cengage Learning; 2015

11. Paudel N. Model Magnetic Materials in the Frequency Domain with an App [online]. COMSOL Blog; January 2016.
    https://www.comsol.com/blogs/model-magnetic-materials-in-the-frequency-domain-with-an-app/. Accessed 25 March 2017.

Appendices

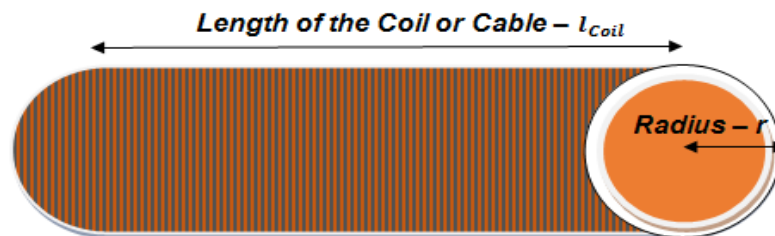## Appendix 1 – Circuit Analogues

Magneto Motive Force [MMF] in a Magnetic circuit:
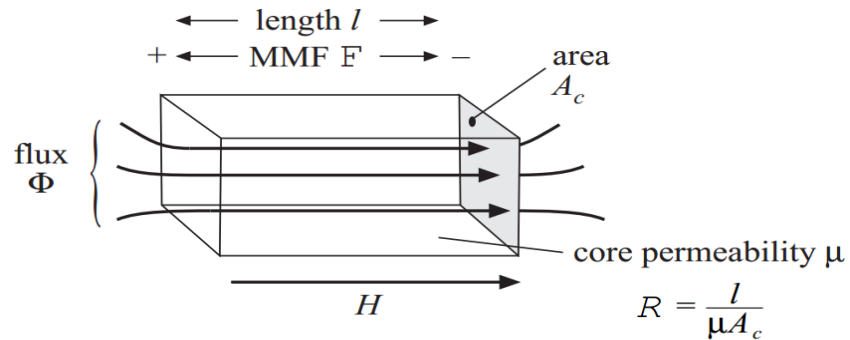
$$MMF \rightarrow F = N * I = H * l_m = \frac{B * l_m}{\mu} \ [A]$$

$$F = \frac{\Phi * l_m}{\mu * A_C} = \Phi * R \ [A]$$

$$Reluctance, \quad R = \frac{l_m}{\mu_0 \mu_r * A_C} = \frac{l_m}{\mu * A_C} \left[\frac{A}{Wb}\right]$$

$$Inductance\ of\ a\ Coil, \quad L = \frac{\mu_r * \mu_0 * N^2 * A_{Coil}}{l_{Coil}} \ [Henry]\ or\ [H]$$

$Here,$
$N \rightarrow Number\ of\ turns\ in\ the\ coil, \quad N = 1\ in\ case\ of\ a\ straight\ wire.$
$\mu \rightarrow Absolute\ Permeability\ of\ Core\ Material.$
$\mu_r \rightarrow Relative\ Permeability\ of\ the\ material\ [dimensionless], \quad \mu_r = 1\ for\ Air.$
$\mu_0 \rightarrow Permeability\ of\ Free\ Space = 1.26 * 10^{-6} \left[\frac{H}{m}\right]$
$A \rightarrow Area\ of\ the\ Coil\ in\ square\ meters = 2\pi r^2 [m^2]$
$l_{Coil} \rightarrow Length\ of\ the\ Coil\ or\ Wire\ in\ meters.$

Appendix 2 – Supplementary Equations

$$Transformation\ Ratio = h = \frac{E_S}{E_P} = \frac{N_S}{N_P}$$

$$Self\ inductance\ of\ a\ coil: L = \frac{\lambda}{I_0} = \frac{N\Phi}{I_0} = \frac{N * B * A}{I_0}\ [Henry, H]$$

$$Mutual\ inductance\ between\ coils: M = \frac{\lambda_{21}}{I_1} = \frac{\lambda_{12}}{I_2}\ [Henry, H]$$

The parallel LC circuit exhibits a resonance at a frequency ω_0 such that the reactance

$$\omega_0 * L = \frac{1}{\omega_0 * C}\ , \qquad \omega_0 = 2\pi f_0$$

$Resonant\ Frequency\ of\ an\ ideal\ resonant\ circuit\ is\ denoted\ by\ f_0,$

$$\omega_0 = \frac{1}{\sqrt{L[H] * C[F]}}\ [Hz], \qquad f_0 = \frac{1}{2\pi\sqrt{L[H] * C[F]}}\ [Hz]$$

$Real\ Resonant\ Frequency, \qquad f_r = \frac{1}{2\pi\sqrt{LC}}\ [Hz]$

$Inductive\ Reactance, \qquad X_L = 2\pi f_r * L = \omega_0 * L\ [\Omega]$

$Capacitive\ Reactance, \qquad X_L = \frac{1}{2\pi f_r * C} = \frac{1}{\omega_0 * C}\ [\Omega]$

$Total\ Circuit\ Reactance, \qquad X_T = X_L - X_C\ or\ X_C - X_L\ [\Omega]$

$Total\ Circuit\ Impedance, \qquad Z = \sqrt{X_L{}^2 + R^2} = R + jX\ [\Omega]$

$Impedance\ of\ a\ parallel\ Circuit, \qquad Z_P = \frac{-j(X_L * X_C)}{X_L - X_C}$

$When\ X_L > X_C\ , the\ circuit\ is\ Inductive.$

$When\ X_C > X_L\ , the\ circuit\ is\ Capacitive.$

$Real\ Resonant\ Frequency\ without\ the\ coupling\ factor - k,$

$$f_r = \frac{1}{2\pi} * \sqrt{\frac{1}{LC} - \left(\frac{R_{DC}}{L}\right)^2}\ [Hz] = f_0 = \frac{1}{2\pi} * \sqrt{1 - \frac{R_{DC}}{L}}\ [Hz]$$

Source:
Inductance and Magnetic Energy, Chapter 11 [online]. Course Notes. MIT Boston, USA: http://web.mit.edu/viz/EM/visualizations/coursenotes/modules/guide11.pdf. Accessed 19 April 2017.

Appendix 3 – Definitions

<u>Permeance</u> - The multiplying or the conducting power for magnetic lines of a force possessed by a given mass of material. It varies with the shape and size of the substance as well as with the inducing force. It is distinguished from permeability, as the latter is a specific quality proper to the material, and expressed as such; the permeance is the permeability as affected by size and shape of the object as well as by its material. Permeance, in general, is the degree to which a material admits a flow of matter or energy. Permeance is usually represented by a curly capital P or capital lambda Λ. It is the reciprocal of reluctance in a magnetic circuit and an analogue of conductance in an electrical circuit.

A **Tesla [T]** is the SI derived unit of the magnetic flux density, commonly denoted as **B**. The magnetic flux density is also known as the "magnetic field B" or the "magnetic induction". One Tesla is equal to one Weber per square meter. A particle carrying a charge of 1 coulomb and passing through a uniform magnetic field of 1 Tesla at a speed of 1 meter per second perpendicular to the said field experiences a force of 1 Newton. As an SI derived unit, the Tesla can also be expressed as 1 [T] = 1 [Wb/m²]

A **Gauss [G]** is the CGS unit of measurement of the magnetic flux density. One gauss is defined as one Maxwell per square centimetre which equals $1*10^{-4}$ [T] or 100 [µT].

$$1 \text{ [T]} = 10^4 \text{ [G]}$$

Source:
Reference and Educational Source [online]. Stands4 LLC.
http://www.definitions.net/definition/permeance. Accessed 20 March 2017.

MUMPS (**MU**ltifrontal **M**assively **P**arallel sparse direct **S**olver) is a software application for the solution of large sparse systems of linear algebraic equations on distributed memory parallel computers. The software implements the multifrontal method, which is a version of Gaussian elimination for large sparse systems of equations, especially those arising from the finite element method.

Source:
https://en.wikipedia.org/wiki/MUMPS_(software)